Bioinspired pH-sensitive riboflavin controlled-release alkaline hydrogels based on blue crab chitosan: Study of the effect of polymer characteristics

Marwa Hamdi, Rim Nasri, S.M. Li, Moncef Nasri

Bioinspired pH-sensitive Riboflavin controlled-release alkaline hydrogels based on blue crab chitosan: Study of the effect of wall polymer characteristics.

Marwa Hamdi [a*], Rim Nasri [a, b], Suming Li [c], Moncef Nasri [a]

[a] Laboratory of Enzyme Engineering and Microbiology, University of Sfax, National Engineering School of Sfax, 3038 Sfax, Tunisia.

[b] Higher Institute of Biotechnology of Monastir, University of Monastir, Monastir, Tunisia.

[c] European Institute of Membranes, UMR CNRS 5635, University of Montpellier, Place Eugene Bataillon, 34095 Montpellier Cedex 5, France.

* Corresponding author: Marwa Hamdi, Laboratory of Enzyme Engineering and Microbiology, University of Sfax, National Engineering School of Sfax, B.P. 1173, 3038 Sfax, Tunisia. **Tel:** 216 25740373 / 216 54186612; **E-mail:** marwahamdi50@yahoo.fr.

1

14 **Abstract**

15   Recently, the application of natural biocompatible polymeric hydrogels for the

16 conception of drug delivery matrices has attracted widespread interest. Thus, in the present

17 study, riboflavin pH-sensitive drug delivery hydrogels were developed based on blue crab

18 chitosan (Cs), via direct dissolution in alkali/urea aqueous solution at low temperatures. First,

19 the effect of Cs characteristics in terms of acetylation degree (AD) and molecular weight (Mw)

20 on the structural, mechanical, thermal, swelling and *in vitro* biodegradation of Cs-based

21 hydrogels were studied. Data from overall analysis revealed that Cs with low AD and high Mw

22 exhibited improved mechanical properties, as evidenced by the compressive and rheological

23 behaviors tests, thermal resistance, swelling behavior and *in vitro* degradation kinetics.

24 However, hydrogels pore sizes were reduced with the AD decrease and Mw increase.

25 Additionally, hydrogels in PBS (pH 5.5) underwent quicker degradation, compared to those

26 immersed in PBS (pH 7.4). In the drug delivery model, the kinetics of Riboflavin release,

27 through the Cs-based hydrogels were monitored. The Riboflavin release exhibited a typical tri-

28 phasic deliverance pattern, with significantly higher released amounts in more acidic systems.

29 Therefore, drug encapsulation within the conceived pH-sensitive Cs-based hydrogels could

30 provide suitable and promoting microenvironment for drugs delivery.

31

32

33   *Keywords:* Hydrogels; Acetylation degree and Molecular weight; Drug controlled-

34 release.

35

36

2

1. Introduction

Hydrogels are three-dimensional hydrophilic polymeric networks with the ability to absorb large amounts of water or biological fluids [1-2]. Because of their high-water content, porosity and soft consistency, they closely simulate natural living tissues, more than any other class of synthetic biomaterials and thus open up many possibilities for applications in biomedical fields [3-5]. Physical hydrogels are distinguished from chemical hydrogels. The network of physical hydrogels is maintained through weak bonds (hydrophobic, hydrogen, ionic) that are not permanent because they are disconnected continuously depending on the medium (pH, temperature, ionic strength). The chemical hydrogels, however, have a network which is maintained by covalent crosslinks providing them a permanent character [6-7].

The high porosity that characterizes hydrogels can easily be adjusted by controlling the density of the crosslinks in their matrix and their affinity to water. Moreover, their porous structure allows to controllably loaded and released drugs [8-9]. The benefits of hydrogels for drug delivery applications include the possibility of controlled and sustained release, which permits a high local concentration of an active pharmaceutical ingredient (drug) to be maintained over a long period of time. The drug can be loaded into a hydrogel, and then released by several mechanisms: controlled release, controlled swelling, chemically controlled release and environmental release [10].

The rate of release can be managed by modifying some factors such as polymer concentration, crosslinking density, and water content. Some «smart» hydrogels have the ability to respond to external stimuli such as pH, temperature, ionic strength, etc., making them excellent site-specific active ingredient in delivery matrices for diseases prevention and treatment [11-12].

Hydrogels are of great interest for other biomedical applications because of the ability to control their swelling, mechanical properties, chemical and physical structures, crosslinking

3

density and porosity. Therefore, hydrogels are frequently used in tissue engineering for cell encapsulation or drug delivery, but as well as wound dressings, bioadhesives and biosensors [13-14]. In fact, hydrogels can serve as templates for directing cell behavior and promoting cell organization. In addition, the biocompatibility of hydrogels has generated a lot of interest in hygiene products, implants and soft contact lenses [15-16].

Advantageously, chitosan can be used in the preparation of hydrogels which serve as a matrix for the incorporation of active agents [17-19]. As part of this research, chitosan obtained by partial deacetylation of chitin was chosen. Chitosan-based hydrogels have shown important advantages in terms of drug delivery, as they allow site-specific and / or time-controlled administration for small and large drugs [17,20]. They offer, furthermore, many benefits, such as improving biosecurity and drug efficacy. Chitosan hydrogels can provide targeted delivery and improved stability of therapeutic agents against physiological degradation [17].

To the best of our knowledge, there is a lack of information in literature regarding the effect of acetylation degree and molecular weight on chitosan-based hydrogels, although several reports describe their developpement and application in particularly the biomedical field. Therefore, the objective of this work was the conception of high strength hydrogels based on chitosans with different acetylation degrees and molecular weights, to assess the effects of these two structural parameters on the properties of the resulting hydrogels. Subsequently, the selected hydrogel was applied for controlled release of Riboflavin with very interesting biological potential, as drug model.

2. Materials and methods

2.1. Materials

Riboflavin was purchased from LOBA CHEMIE (India) and the other used chemical reagents from commercial sources were of analytical grade and employed without further purifications.

4

2.2. Chitosans preparation and purification

Chitosans (Cs) from blue crab *Portunus segnis* shells were prepared in our laboratory, as described in our previous study [21]. Briefly, Cs with different AD were obtained through chitin N-deacetylation with NaOH 12.5 M at a w/v ratio of 1/10 at 140 °C, for 2, 3 and 5 h and produced Cs were named Cs I, Cs II and Cs III. After filtration, Cs was washed to neutrality and then dried for 12 h at 50 °C. Based on the nuclear magnetic resonance (^{13}C NMR) analysis, ADs of 17%, 13% and 8% were reached for Cs I, Cs II and Cs III, respectively. Further, Cs were characterized by size exclusion chromatography (SEC-HPLC) and average molecular weights (Mw) of 125 600, 118 900 and 115 000 g mol^{-1} were obtained for CsI, CsII and CsIII, respectively.

To generate Cs with different Mw, Cs, at different ADs, were hydrolyzed with Cellulase (10 U/g chitosan) in 0.5 N acetate-bicarbonate buffer (pH 5.2) at 55 ° C, for 1 and 3 h, as described by Chang *et al.* [22] with slide modifications. The Cs obtained are lyophilized and analyzed to study the evolution of their molecular mass. The respective Mw were reported in **Table S1**.

Subsequently, Cs were purified according to the method described by Qian and Glanville [23]. Thus, crude Cs (6 g) was dissolved in 600 ml of HCl 0.1 M under stirring overnight at a temperature of 40 °C. The acidic solution was vacuum filtered to remove insoluble particles. Cs was then precipitated with NaOH 0.5 M under continuous stirring until approximatively pH 8.5. Thereafter, 6 ml of 10% (w/v) sodium dodecyl sulfate (SDS) was added to the suspension and the mixture was heated at 95 °C for 5 min. After cooling at room temperature, the pH was adjusted to 10.0 with 0.5 M NaOH. The mixture was vacuum filtered and the hydrated Cs was washed 5 times with 600 ml of deionized water at 40 °C. A solution of barium chloride was used to confirm the absence of residual SDS in the filtrate. Finally, the obtained purified Cs were lyophilized, milled to powder and then sieved.

5

2.3. Conception of blue crab chitosan-based hydrogels

Hydrogels were prepared based on the freezing/thawing approach described by Duan *et al.* [5]. Briefly, Cs, derived from the action of Cellulase, were dissolved in an alkaline solution, widely used for the dissolution of cellulose and chitin, consisting of 4.5 wt. % LiOH, 7.5 wt. % KOH and 8.5 wt. % urea. Then, the reaction mixtures were maintained at -30 °C until complete freezing, followed by a thawing step at 20 °C under vigorous agitation, until a clear and transparent solution of Cs was obtained. After removal of air bubbles by centrifugation at 5000 ×g for 15 min at 4 °C, the prepared solutions were maintained at 60 °C for 1 h (solvent evaporation technique), promoting the formation of Cs physical gels. After exhaustive washing with Milli-Q water, to remove the residual alkali/urea solution, prepared hydrogels were immersed in an ethanol solution (100%) for 3 days to improve the resistance of the gels [24].

Foremost, Cs-based hydrogels with different AD and Mw were prepared at a concentration of 3% (w/v) [24], to study the effect of these two parameters on the structural, mechanical and rheological features of elaborated hydrogels. The corresponding code to each hydrogel was recorded in **Table S2.** Subsequently, an optimization of the ideal concentration for the formation of Cs-based hydrogels was performed. Accordingly, different concentrations were used, namely 1%, 2%, 3%, 4% and 5% of Cs, and the obtained hydrogels were characterized.

2.4. Blue crab chitosan rheological behavior in the alkali/urea aqueous solution

To study the stability of the Cs in alkali/urea system, hydrogels (15 mm of diameter × 1 mm of thickness) rheological and gelation behaviors were investigated with dynamic viscoelastic measurements. For all the experiments, a rheometer apparatus (Physica MCR, Anton Paar, GmbH, France) equipped with a plate-plate measuring geometry (25 mm diameter, 0.1 mm gap) was used. Oscillatory measurements of the storage modulus (G′) and loss modulus (G″) were carried out under a strain sweep from 0.1% to 1000% at 37 °C with a frequency of 1

6

137 Hz. Thermo-viscoelasticity properties in a ramp temperature from 20 to 80 °C was investigated,

138 under constant frequency (1 Hz) and strain (1%), at a heating rate of 2 °C/min. A solvent trap

139 was applied to prevent water evaporation when heating. The data were analyzed with Rheoplus

140 software from Anton Paar.

2.5. Analytical methods

141

2.5.1. Hydrogels microstructure

142

143 The cross-section of Cs-based hydrogels was studied using scanning electron microscopy

144 SEM (Hitachi S4800), at an angle of 90° to the surface, at different magnifications. Prior to

145 imaging their cross-section, hydrogel samples were lyophilized, sectioned and fixed on the

146 SEM support using double side adhesive tape, and observed up to a 2000 x magnification, under

147 an accelerating voltage of 2.0 kV and an absolute pressure of 60 Pa, after being sputter coated

148 with a 5 nm thick gold.

2.5.2. Moisture content of Cs-based hydrogels

149

150 The water content was determined according to the methods described by AOAC (2000)

151 [25]. The water content of the elaborated hydrogels was measured, in triplicate, by drying about

152 100 mg of each sample in an oven at 105 °C until the dry weight of the sample was reached

153 (constant weight). Weights before and after drying were measured. The moisture content of

154 hydrogels was determined by measuring the mass loss of each film in triplicate and expressed

155 as follows:

$$\text{MC (\%)} = \frac{W_0 - W_1}{W_0} \times 100$$

156

157 where W_0 and W_1 are the respective masses (g) of hydrogels before and after drying at 105 °C.

2.5.3. Swelling rate of hydrogels

158

159 The swelling test was performed on pieces of hydrogels with masses of 20-30 mg. The

160 samples were immersed in phosphate-buffered saline (PBS) at 37 °C and after 24 h of

7

161 incubation, the samples were removed, oven-dried and the masses were measured again [26].

162 The swelling rate (SR), repeated three times, was calculated as follows:

163
$$SR\ (\%) = \frac{M_s - M_d}{M_d} \times 100$$

164 where SR is the swelling rate (%), M_d is the mass (g) of the oven-dried hydrogel and M_s is the

165 mass (g) of the swollen hydrogel.

166 2.5.4. Infrared spectroscopy analyses

167   The prepared Cs-based hydrogels FT-IR analysis was performed by means of a

168 spectrometer (Agilent Technologies, Carry630 series) with an attenuated reflection accessory

169 (ATR) containing a diamond/ZnSe crystal, at room temperature (25 °C). Spectra were recorded

170 in the spectral range frequencies of 650-4000 cm^{-1}, with 32 scans of interferograms and a

171 resolution of 4 cm^{-1}. Prior to analysis, FT-IR spectrometer was calibrated via a background

172 spectrum recorded from the clean and empty diamond for each spectrum. Data analysis and

173 treatment were carried out using the OMNIC Spectra software (ThermoFisher Scientific).

174 2.5.5. X-ray diffraction studies

175   To further investigate the structural characteristics of the prepared hydrogels, XRD

176 patterns were recorded using an X-ray diffractometer (D8, Advance Bruker XRD

177 diffractometer, Germany). Ni-filtered Cu Kα radiation (k = 1.5406 ˚A) was used to record the

178 X-ray patterns. The relative intensity was recorded in the scattering range 2θ of 5–50° with a

179 step size of 0.02° and a counting time of 5 s/step, with an error of ±1°.

180 2.5.6. Thermal properties of blue crab chitosan-based hydrogels

181   Thermogravimetric analysis (TGA Q500 High Resolution, TA Instruments), operating

182 under nitrogen flow, was used to study the thermal stability of Cs-based hydrogels. The mass

183 change of a sample as a function of temperature augmentation is the basis of TGA, and the

184 progressive change in mass (%) as function of temperature, is recorded. Cs-based hydrogels,

8

185 initially about 4 mg, were heated from 25 to 700 °C at a heating rate of 20 °C/min and constantly

186 measured with an accuracy of 0.01 mg. Cs-based hydrogel thermograms were subsequently

187 analyzed using TA Universal V4.5A software.

2.5.7. Evaluation of hydrogels mechanical properties

189 Hydrogel compression tests were carried out using the DMA50 (Dynamic Mechanical

190 Analyzer) universal testing machine (Metravib, Brand of ACOEM, France) at a temperature of

191 25 °C and a compression speed of 1 mm/min. Samples were compressed at 10%, 20%, 30%,

192 40%, 50% and 60%, and then reverted at the same speed of 1 mm/min, to obtain the stress-

193 strain curves for gels' compression-recovery. The dimensions of the hydrogel specimens

194 (parallelepiped) for compression tests were 10 mm × 5 mm × 5 mm (based on the apparatus

195 requirements). The stress-strain curve hysteresis was recorded and treated by the instrument

196 software.

2.5.8. Hydrogels *in vitro* degradation test

198 Cs-based hydrogels *in vitro* biodegradation study was monitored through the gravimetric

199 method described by Qu *et al.* [27]. Briefly, hydrogels (approximatively 100 mg) were

200 immersed in 10 ml of phosphate buffer saline (PBS) at pH 7.4 (physiological microenvironment

201 simulation) and pH 5.5 (acidic microenvironment), at 37 °C and under gentle shaking

202 (approximatively 100 rpm). Thereafter, hydrogel samples were removed, at each desired

203 interval time, washed with Milli-Q water to remove the excess of salinity, oven-dried for 48 h

204 at 60 °C and then weighed. The remaining weight of hydrogels (%) was calculated based on the

205 following equation:

$$\text{Remaining weight ratio (\%)} = \frac{M_t}{M_i} \times 100$$

207 where M_t is the remaining hydrogels dry weight after degradation at each selected time interval

208 and M_i is the initial hydrogels dry weight.

9

2.6. *In vitro* riboflavin loading and release kinetics

The amount of riboflavin incorporated in hydrogels was studied. Briefly, wet Cs-based hydrogel (30 mg) were suspended in 10 ml of riboflavin solution (1-5 g/l) in dark at 5 °C for 48 h. The riboflavin entrapment efficiency and loading capacity by the hydrogels were determined considering the derivative thermogravimetric (DTG) thermograms [28], by subtracting the amount of riboflavin in the supernatant from the total amount applied [24]:

$$\text{Riboflavin loading capacity (\%)} = \frac{\text{Mass of loaded riboflavin}}{\text{Mass of hydrogel samples}} \times 100$$

$$\text{Riboflavin entrapement efficiency (\%)} = \frac{\text{Mass of loaded riboflavin}}{\text{Mass of initial riboflavin}} \times 100$$

Regarding the riboflavin release studies, loaded hydrogel samples (30 mg) were subsequently incubated in 10 ml of aqueous HCl and NaCl (0.1 M) with different pH values (pH 2.0, 4.5 and 7.4) at 37 °C, with stirring. At each time interval, an aliquot of the supernatant (2.5 ml) was withdrawn and replaced by fresh medium at the same volume. The amount of released riboflavin was determined spectrophotometrically, considering the cumulative amount of riboflavin in each of the release system. The amount of riboflavin was estimated using a UV-visible spectrometer (Agilent Technologies, Carry 630 series) at 450 nm on the basis of a riboflavin calibration curve (**Data not shown**). All studies were performed in duplicate and the average values were reported.

2.7. Statistical analysis

Statistical analyses were performed with SPSS ver. 17.0, professional edition (SPSS, Inc., Chicago, IL, USA) using ANOVA analysis at a p-value < 0.05. A standard deviation at the 95% confidence level was used to compare all parameters analyzed for the different hydrogels All assessments were repeated three times and average values with standard deviation errors were reported.

10

3. Results and Discussion

3.1. Microstructure analysis of Cs-based hydrogels

Since understanding biomaterials functional properties is based on their structure knowledge, the examination of Cs-based hydrogels microstructure, reflecting polymer and molecules interactions, is required [29].

SEM images showing the pore microstructure (cross section) of Cs-based hydrogels, with different AD and Mw, are displayed in **Fig. 1**. The pore size of the prepared hydrogels changed in the range of $1 \sim 6$ µm and became bigger and bigger as the Cs AD increased, with more compact distribution. For example, pore size values of ~ 1 µm for CsIII-0 based hydrogel (**Fig. 1G**), 2 µm for CsII-0 based hydrogel (**Fig. 1D**) and 3 µm for CsI-0 based hydrogel (**Fig. 1A**) were reached, suggesting that lower AD allowed the preparation of a more well-organized network structure, which could contribute to mechanical support [30].

It was found likewise that the hydrogel pore size had the tendency to decrease with the increase of Cs Mw. Indeed, the pore size (approximatively 4 µm; **Fig. 1I**) of CsIII-3 based hydrogel, showing a microstructure, filled with larger interconnected pores, was about twice of that for CsIII-1 based hydrogel (approximatively 2 µm; **Fig. 1H**), which could lead to modulations in Cs-based hydrogels swelling and drug release behaviors [17].

In another aspect, overall Cs-based hydrogels, regardless Cs AD and Mw, as shown in **Fig. 1**, the formed hydrogels network revealed a uniformly distributed porous three-dimensional architecture, with, to variable extend, a roughness matrix surface. The pores interconnected in a recurrent style inside the hydrogels network affords a suitable medium flow and drug transport channels, being therefore appropriate for drug delivery [26,31].

3.2. Hydrogels moisture content determination

Moisture content (MC) of Cs-based hydrogels, reported in **Table 1**, revealed that values decreased with the decrease of the AD, reaching 82%, 81% and 79%, for CsI-0 (AD=17%),

11

257 CsII-0 (AD=13%) and CsIII-0 (AD=8%) based hydrogels, respectively (p<0.05). however,

258 considering Cs Mw, MC values were found to be strengthened with the decrease of Cs Mw.

259 Indeed, regarding an AD of 8% (CsIII), hydrogels MC rates of 79.90%, 80.26% and 81.83%

260 were reached with respective Mws of 115 kDa (CsIII-0), 78.43 kDa (CsIII-1) and 16.04 kDa

261 (CsIII-3), probably due a decrease of crosslinking density [5]. In fact, hydrogels are systems

262 known for their remarkable water-holding capacity during their preparation, and the water

263 content is one of the most features that distinguishes hydrogels from other biomaterials. Their

264 water-rich structure facilitates, indeed, the transport of nutrients and molecules between the

265 external environment and the hydrogel, which allows to mimic the function of cells in the body

266 [9].

267 Consequently, it could be proposed that the increase of CS MW, besides the decrease of

268 its AD, as well as Cs-based hydrogels soaking in ethanol solution (100%), allowed the decrease

269 in Cs-based hydrogels water content, and thereby, reducing pore sizes [24], which was

270 consistent with SEM data. This finding seems to be beneficial for Cs-based hydrogels

271 mechanical properties enhancement.

272 **3.3. Evaluation of Cs-based hydrogels swelling properties**

273 As an absorbent matrix, the degree of swelling of a hydrogel is a key parameter that is

274 closely related to the ability of hydrogels to release active ingredients [32]. Swelling is defined

275 as a continuous transition process from the solvent-free glassy state or partially rubbery state to

276 a relaxed rubbery solvent containing state. The solvent infiltration and the elastic contraction

277 from the network strain, as two opposite forces, create a skirmish in the swelling process, which

278 reaches the equilibrium, when they reach a dynamic balance [33]. In this context, the effect of

279 Cs AD and Mw on Cs-based hydrogels swelling ratio (SR) was studied and results are recorded

280 in **Table 1**.

281   Results display that Cs-based hydrogels water absorption capacity was found to be

282 dependent to the Cs AD and Mw. Indeed, SR values increased with the decrease of Cs AD as

283 well as the decrease in its Mw. For example, hydrogels developed with CsI (CsI-0; AD=17%)

284 exhibited SR value of 13.59±0.45 g/g, compared to CsIII-0 based hydrogel, prepared with lower

285 AD Cs (CsIII-0; AD=8%), with SR exceeding 18 g/g (**Table 1**). Moreover, regarding CsIII-

286 based hydrogel, respective SR values of more than 18 g/g, 22 g/g and 26 g/g were reached with

287 hydrogels prepared with GCsIII-0 (115 kDa), GCsIII-1 (78.43 kDa) and CsIII-3 (16.04 kDa).

288   It is well known that the swelling properties of hydrogels depend on the hydrophilic

289 nature of polymeric chains and the nature of bonds inside the matrix structure. Thus, it is

290 possible to deduce that the decrease of Cs AD, and thereby, the increase of the -NH_2 groups

291 number, allowed the improvement of the hydrophilicity of the elaborated hydrogels, favoring

292 their interaction with water molecules [34,35]. In addition to the polarity of the hydrogels, the

293 degree of crosslinking and hydrogels porosity were found to well correlate with the ability of

294 Cs-based hydrogels to absorb water [12,27].

3.4. Hydrogels spectroscopic characterizations

3.4.1.   FT-IR analysis

297   The FT-IR spectra of Cs-based hydrogels were shown in **Fig. 2**. Compared to the polymer

298 powder [21], characteristic Cs absorption bands at 3417 cm^{-1}, 1627 cm^{-1}, 1544 cm^{-1}, 1407 cm

299 $^{-1}$ and 1020-1097 cm^{-1} linked to the -OH, amide I groups (-C = O), amide II (-NH_2), -CH and

300 glycoside rings, respectively, were noted to be rearranged. Indeed, the N–H peak in the FT-IR

301 spectra of the Cs-based hydrogels was found to be shifted significantly to higher wavenumbers

302 overlapping with the peak of the O–H stretching vibrations. The peak at 3500–3200 cm^{-1}

303 straitened, and revealed the tendency to break into several small peaks, demonstrating the

304 weakening of the inter- and intra-molecular hydrogen bonds and the occurrence of some

305 reactions on the two groups [34-39].

13

306   The peak of the amide I group weakened remarkably and almost disappeared, indicating

307   that concentrated alkali has reacted with the acetyl amino group of Cs [38,39]. Moreover, new

308   stretch vibration absorption bonds appeared at about 3264 cm^{-1}, 2500 cm^{-1} and 785 cm^{-1},

309   indicating that the alkali/urea aqueous solvent affected the structure of Cs to some extent.

310   Indeed, active hydroxyl group of Cs reacted with the concentrated alkali, leading thereby to the

311   destruction of the native hydrogen bonds of Cs effectively and making Cs highly swell or even

312   dissolve in the alkali solution.

313   These findings confirmed further during the dissolution process, alkali not only reacts

314   with the hydroxyl group, but also with the acetyl amino group of Cs, leading to the weakening

315   of the amide I peak ascribed to acetyl amino group [40,41]. Moreover, The FT-IR spectra of all

316   Cs-based hydrogels are quite similar, regardless Cs AD and Mw, accounting for the stability of

317   Cs in the alkali/urea aqueous solution system [24, 42,43].

318   **3.4.2. XRD patterns study**

319   To further clarify the structural changes in the Cs matrix, during dissolution in the

320   alkali/urea aqueous system and gelling, and regarding the effects of Cs Mw and AD, XRD

321   patterns of Cs-based hydrogels were studied and compared to the polymer powder profiles (**Fig.**

322   **3**). X-diffractograms of Cs-based hydrogels revealed marked differences in the molecular state.

323   Indeed, diffraction peaks nearby 13.1° and 21.3°, attributed to (020) and (110) planes of Cs,

324   respectively, were detected, reflecting the semi-crystalline structure of Cs [21,44]. The major

325   peaks at $2\theta = 37.7°$, $34.32°$, $32.4°$ and $28.9°$ observed in the X-diffractograms could be

326   attributed to the alkali (LiOH) used for the dissolution of Cs [45].

327   As shown in **Fig. 3**, the Cs-based hydrogels displayed the characteristic diffraction

328   patterns of both Cs and alkali at the same time. However, the crystallinity of the physical Cs-

329   based hydrogels clearly diminished in comparison with that of Cs powder, where the above

330   mentioned initial characteristic peaks became broader and weaker, depending on Cs AD and

14

827
828
829
830
831
832
833
834
835
836
837
838
839
840
841
842
843
844
845
846
847
848
849
850
851
852
853
854
855
856
857
858
859
860
861
862
863
864
865
866
867
868
869
870
871
872
873
874
875
876
877
878
879
880
881
882
883
884
944

331 Mw. In fact, convenient with the SEM images, the crystallinity of Cs-based hydrogels decreased

332 with the increase of Cs AD (CsI-0 based hydrogel) and the decrease in its Mw (Cs-1 and Cs-3

333 based hydrogels), suggesting a transition from a crystalline structure to an amorphous state

334 during the dissolution and the gelling process [46,47]. This result strongly confirmed that Cs

335 solubility was related to its crystallinity.

336 With the aid of alkali solution and the freezing to -30 °C, water molecules diffuse in the

337 Cs macromolecular chain. The subsequent thawing and stirring steps during hydrogels

338 preparation process are beneficial for the dissolution of Cs, as the intra- and inter-molecular

339 hydrogen bonds of Cs would be broken during dissolution, leading to the loss of crystallinity

340 [48,49].

341 The dissolution of Cs in the alkali aqueous system begins at the amorphous side with a

342 loose structure at first, and afterwards reaches the crystal zone with a rather thicker construction

343 and low temperature. This exhibits a crucial role in the Cs crystalline configuration destruction

344 [26,50]. Meanwhile, overall findings proposed that the chemical structure of Cs was relatively

345 stable in the alkali/urea aqueous solution [5,24].

346 **3.5. Cs AD and Mw affected based hydrogels thermal properties**

347 Thermal stability/degradation behavior of Cs-based hydrogels, with respect to their AD

348 and Mw, was studied, and results in terms of TGA and derivate (DTG) thermograms, are shown

349 in **Supplementary data Fig. S1**. The thermal decomposition data in terms of the corresponding

350 degradation temperatures, the weight loss (Δw) and the residue (**R**), were estimated (**Table 2**).

351 Based on data from the obtained TGA thermograms, the thermal decomposition profiles

352 of the overall Cs-based hydrogels exhibited a similar weight loss process in the temperature

353 range of 20–800 °C, indicating the polymer pyrolysis, and characterized by three major phases

354 (**Supplementary data Fig. S1**), typical fingerprint of Cs thermal decomposition [32].

355   The first phase corresponded to a weight loss of 6% (CsIII-0 based hydrogel) to 19%

356 (CsI-3 based hydrogel), apparently resulted from evaporation of adsorbed water by Cs at a

357 temperature (Td1) range from 28-46 °C to 129-158 °C, reaching its maximum mainly below

358 130 °C, expect for the CsIII-0 based hydrogel (133.54 °C). The different content of bound and

359 unbound water in the hydrogels could explain the observed difference in onset temperature [51].

360 Indeed, in line with data from the SEM analysis and results above mentioned, CsIII-0 based

361 hydrogel exhibited higher onset temperature as a result of more strongly bound water, related

362 to a more homogeneous network structure. However, less uniform network with macro-phase

363 separation like structure, observed in hydrogels based on CsI-3, was found to responsible of

364 more unbound water in the based hydrogel structure [28,48].

365   Considering the DTG curves, the temperature, at which the decomposition process was

366 the shrillest, was revealed by the weight loss peak (**Supplementary data Fig. S1**). In the range

367 the third phase of Cs-based hydrogels pyrolysis process (200-550 °C), where higher ΔW were

368 reached, peaks located at temperatures of 268.81, 266.09 and 261.55 °C, were found for the

369 CsI-0, CsI-1 and CsI-3 based hydrogels, respectively, whereas those found at 279.71, 274.26

370 and 273.35 °C were related to the CsIII-0, CsIII-1 and CsIII-3 based hydrogels, respectively

371 (**Table 2**). Thus, polymers pyrolysis temperature differences are mainly assigned to the

372 macromolecular interaction, crystallinity index, or orientation. The TGA results proved that

373 CsIII-0 based hydrogel was reorganized in more well-ordered network structure, during the

374 dissolution in the alkali/urea system at low temperatures and the regeneration process in

375 ethanol, ensuing a rather high crystallinity and more homogeneous architecture. Finally,

376 residual decomposition reactions leading to the total degradation of the Cs ring in the hydrogels

377 was found to be around 550 °C [52].

378   Regarding the residual mass (R) of the prepared hydrogels, values were found to decrease

379 with the decrease of the Cs Mw and the increase of its AD, with values of 33.70% (CsI-0 based

16

945
946
947
948
949
950
951
952
953
954
955
956
957
958
959
960
961
962
963
964
965
966
967
968
969
970
971
972
973
974
975
976
977
978
979
980
981
982
983
984
985
986
987
988
989
990
991
992
993
994
995
996
997
998
999
1000
1001
1002
1062

380 hydrogel), 30.59% (CsI-1 based hydrogel) and 29.88% (CsI-3 based hydrogel). Considering

381 CsII-based hydrogels, R values of 34.34%, 33.05% and 29.58% were reached for the CsII-0,

382 CsII-1 and CsII-3 based hydrogels, respectively. R values of 47.69%, 40.53% and 38.68% were

383 noted for CsIII-0, CsIII-1 and CsIII-3 based hydrogels, respectively (**Table 2**). Accordingly, it

384 could be concluded that thermal stability of the Cs-based hydrogels is positively correlated with

385 its AD and disproportionate to its Mw. Moreover, as discussed earlier, TGA findings confirmed

386 that the increased stability of the Cs-based hydrogels was due to increasing macromolecular

387 chains crosslinking [28,32].

3.6. Hydrogels mechanical properties as affected by Cs structural parameters

3.6.1. Rheological behavior

390 The rheological properties of Cs-based hydrogels, storage modulus (G′) and loss modulus

391 (G″), were shown as a function of strain at 37 °C (**Fig. 4A-C**). Independently of Cs AD or Mw,

392 Cs-based hydrogels displayed higher elastic behavior (G′>G″) than the viscous behavior

393 (G′<G″), suggesting a distinctive feature of a strong hydrogel.

394 Since the elasticity of the sample, defined as the stored energy due to the elastic

395 deformation, is reflected by the storage modulus G′, the higher the G′ value is, the tougher

396 against distortion the hydrogel is [33]. **Fig. 4A-C** shows that for all the Cs-based hydrogel

397 samples, the moduli (G′ and G″) fluctuated slightly with deformation in the test strain range of

398 500%. Comparing the hydrogel samples, for CsIII-0 based hydrogel, the G′ (more than 130

399 kPa) was found to be significantly higher than that of CsII-0 (more than 82 kPa) and CsI-0

400 (more than 35 kPa) based hydrogels. Additionally, for CsIII-1 (G′ about 30 kPa) and CsIII-3

401 (G′ more than 17 kPa) based hydrogels, the G′ values were significantly lower than that of

402 CsIII-0 based hydrogel (p<0.05). The same tendency was detected with the other hydrogels

403 based on CsII (AD of 13%) and GCsI (AD of 17%).

17

404 Before hydrolysis, G' of Cs-based hydrogels, independently of Cs AD, was four times

405 more than the value of Cs-1 and Cs-3 based hydrogels, thus, the creation of a more stable

406 network, leading to a greater maximum storage modulus G'.

407 This finding could be mainly assigned to the stronger interactions of Cs macromolecular

408 chains, with high average molecular weight, than medium and lower average molecular weights

409 Cs (Cs-1 and Cs-3, respectively). The formation of covalent bonds between the Cs and the

410 alkali/urea system, allowed thereby remarkably the enlargement of the strength of hydrogels

411 and the enhancement of their mechanical properties [5,27,33].

412 Data of gradually decreasing storage modulus G' of the hydrogels, with the decrease of

413 Cs AD and the increase of the Mw, were consistent with the gradually increasing SR results

414 above described (**Table 1**), further, principally ascribed to the progressively hydrogels

415 crosslinking density diminishing [24,53].

416 As displayed in **Fig. 4A-C**, it is likewise found that an increase in the deformation, more

417 than 500%, was associated with loss/viscous modulus G" enlargement and storage/elastic

418 modulus G' decline, as the network movement increased [54], demonstrating that at higher

419 strains elastic flow of the gel network decreased. However, unlike the G' profile, the gel-sol

420 transition strain value was found not significantly influenced with the Cs AD or Mw.

421 In another aspect, there was found no remarkable difference of Cs-based hydrogels

422 rheological properties as function of the temperature (**Supplementary data Fig. S2**). Indeed,

423 interestingly, as the temperature increased from 10 to 60 °C, there was no change of G' and G"

424 of the hydrogel samples. Therefore, physical Cs-based hydrogels, based on the dissolution in

425 the alkali/urea aqueous system at low temperatures, exhibited stable rheological properties

426 against temperature, regardless the Cs AD or Mw.

427 Such rheological behaviors of Cs-based hydrogels, with interesting elastic and solid

428 characteristics, showed the attendance of a promising material for tissue engineering application

429 [55]. Moreover, rapid drug loss prevention and better sustained release properties could be

430 potentially provided by high gel strength and short gelation time of the hydrogel, as obtained

431 with the Cs-based hydrogels [56].

432 **3.6.2. Compressive study**

433 Considering the bone tissue engineering, the mechanical properties of biomaterials like

434 hydrogels are design features of priority [57,58]. To have additional insight into the mechanical

435 behavior of Cs-based hydrogels, compressive properties were evaluated by exposing wet gels

436 to compression testing and the stress *vs.* strain compressive curves, with different Cs ADs and

437 Mws, are shown in **Fig. 4D-F**. Mechanical experimental outcomes display that under

438 compression, the compressive strength of the Cs-based hydrogel samples increased with the

439 increase in compressive strain for all hydrogel formulations. More particularly, the compressive

440 stiffness of Cs-based hydrogels increased concomitantly with the increase of the applied

441 compressive strain in the range of 5-7% deformation, and then sticked to rise but in a slower

442 manner, indicating that the Cs-based hydrogels were sturdy and ductile.

443 The order of the mechanical properties was found as: CsIII>CsII>CsI. Indeed, when the

444 Cs AD increased from 8% (CsIII based hydrogel) to 17% (CsI based hydrogel), the fracture

445 stress values of the Cs-based hydrogels decreased to 0.35 MPa for CsI-0 based hydrogel, while

446 values of 0.49 MPa and 0.71 MPa were reached with CsII-0 and CsIII-0 based hydrogels,

447 respectively ($p<0.05$). CsIII-3 based hydrogel was found to endure 40% deformation, whereas

448 CsII-3 and CsI-3 based hydrogels were capable to bear only 35% and 30% deformation,

449 respectively, because of the decrease in the physical crosslink density of the Cs network (**Fig.**

450 **4D-F**), suggesting a relatively high strength for CsIII based hydrogel, with the highest

451 macromolecular interactions, the most stable network and the smallest pore size [39,59].

452 In another side, the increase in Cs Mw was found to result in a significant enhancement

453 in ultimate compressive stress and strain of fracture ($p<0.05$). In fact, hydrogels developed

19

454 based on low Mw Cs (CsIII-3, CsII-3 and CsI-3) exhibited mechanical stiffness of more than

455 0.29 and 0.27 and 0.11 MPa, respectively. However, ultimate stress modulus increased by 2

456 and more than 3-folds for medium (CsIII-2, CsII-2 and CsI-2) and high (CsIII-0, CsII-0 and

457 CsI-0) Mw Cs, respectively (**Fig. 4D-F**). Interestingly, with ADs less than 13% (CsII and CsIII),

458 even with medium Mw, based hydrogels kept the structural integrity and stability without

459 evidences of any sign of fracture and could recover by themselves subsequently to external

460 pressure removal. This finding strongly demonstrated that the synthesized hydrogel exhibited

461 interesting mechanical properties, thanks to stiffer chains resulting in stronger pore wall,

462 allowing gels thereby to undergo more intense external forces and conditions [33,51,57].

463 These mechanical data were further consistent with the crystallinity results (**Fig. 3**) and

464 the microstructure of the Cs-based hydrogels (**Fig. 1**).

465 **3.7. Hydrogels *in vitro* degradation behavior**

466 The degradation behavior, based on the weight loss system, was monitored in PBS at pH

467 values of 7.4 and 5.5 to simulate the physiological and acidic microenvironments, respectively.

468 Significant differences (p<0.05) were observed, in terms of Cs AD and Mw, considering

469 degradation kinetics over 7 days of incubation time (**Fig. 5**). Additionally, the degradation

470 behavior patterns were peculiar after immersion under simulated physiological (pH 7.4) and

471 acidic (pH 5.5) conditions at 37 °C. However, independently of the swelling conditions and Cs

472 characteristics (AD and Mw), more than 75% of the initial mass was preserved (**Fig. 5**).

473 Independently of Cs characteristics, hydrogels, in PBS of pH 5.5, underwent most quicker

474 degradation, compared to samples immersed in PBS of pH 7.4. For example, CsIII-0 based

475 hydrogel retained about 91% mass in acidic microenvironment (**Fig. 5A**), and more than 95%

476 mass in PBS pH 7.4 (**Fig. 5B**), within 4 days. Qu *et al.* [27], based on the morphology of the

477 hydrogels observed under SEM images, proved that differences in degradation behavior could

478 be ascribed to an increase in pore sizes, which increased significantly after immersion in PBS.

20

1181
1182
1183
1184
1185
1186
1187
1188
1189
1190
1191
1192
1193
1194
1195
1196
1197
1198
1199
1200
1201
1202
1203
1204
1205
1206
1207
1208
1209
1210
1211
1212
1213
1214
1215
1216
1217
1218
1219
1220
1221
1222
1223
1224
1225
1226
1227
1228
1229
1230
1231
1232
1233
1234
1235
1236
1237
1238
1298

479   This increase was more pronounced for hydrogels swollen in acidic conditions (PBS of pH 5.5),

480   that in the long term, could quick the degradation of hydrogels, due to protonation of chitosan

481   amino groups. Indeed, pKa value of D-glucosamine residue is about 6.2~7.0. Subsequently,

482   macromolecular chains bonding become brittle, leading to the hydrogel's networks destruction

483   and decomposition.

484   As expected, Cs-based hydrogels with higher AD and lower Mw exhibited a faster weight

485   loss after immersion in both media (PBS of pH 5.5 and pH 7.4). After incubation for 7 days,

486   the attained mass losses were about 20%, 22% and 25% for CsI-0, CsI-1 and CsI-3 based

487   hydrogels, respectively, while, CsIII based hydrogels still retained more than 80% (CsIII-0),

488   78% (CsIII-1) and 75% (CsIII-3) of their original weight, under swelling in pH 5.5 PBS, after

489   7 days of incubation time (**Fig. 5A**). These findings corroborate well and directly with the pore

490   diameters distribution based on the SEM images, the swelling and mechanical behaviors of

491   prepared hydrogels and the observed crystallinity data. These results proposed that Cs-based

492   hydrogels, with good biodegradability and interesting stability in PBS, could exhibit potential

493   and promising application in tissue engineering [12,55,59].

494   During the last decades, smart biomaterials as oral administrative drug carriers attracted

495   day-by-day the attention of researchers in the biomedical field [60]. Therefore, Cs-based

496   hydrogels developed in the present study could be considered as porous promising pH-sensitive

497   biomaterial, with sufficient space for the diffusion of small molecules and drugs, and exercising

498   drug release management capability.

499   **3.8. Optimization of blue crab chitosan concentration for hydrogels construction**

500   An optimization of the ideal concentration of Cs for the formation of hydrogels was

501   performed on the basis of the compressive property test and storage modulus determination.

502   CsIII-0 based hydrogel was selected for the optimization of Cs concentration study, considering

503   its appropriate structural architecture, swelling behavior and mechanical strength.

21

504   Mechanical properties of the different Cs-based physical hydrogels, considering the

505 compression stress-strain diagrams are illustrated in **Fig. 6A**. The application of a compressive

506 force on the hydrogels made it possible to obtain two phases. At low deformation values (around

507 5%), an elastic (reversible) deformation was observed as a straight line where the deformation

508 was proportional to the stress. Beyond 5%, the stress increased slowly, giving evidence of a

509 plastic deformation (irreversible) occurrence, due to the breaking of the bonds or rearrangement

510 of the structure [12].

511   As displayed in **Fig. 6A**, hydrogel compressive strength was improved with the increase

512 of Cs concentration from 0.24 MPa for 1% of Cs to more than 0.48 MPa for hydrogel at 4% of

513 Cs. The Cs solution at 1% concentration was found to be not able to form solid physical

514 hydrogel and the hydrogel prepared was too weak to be handled and analyzed, mainly due to

515 the rather low polymer amount. Indeed, the formed hydrogel was fractured under compressive

516 deformation less than 30%. However, hydrogels prepared with more than 2% Cs were already

517 relatively rigid and resistant. Further, data revealed that fracture resistance of all hydrogel

518 samples was found to be Cs concentration dependent, where 2% Cs-based hydrogel tolerated

519 more than 45% of compressive deformation to be fractured, whereas, 50% of compressive

520 deformation was not sufficient to induce hydrogels fracture at more than 3% Cs (**Fig. 6A**).

521 However, 5% Cs-based hydrogel exhibited a significant decrease in the compressive stress to

522 around 0.4 MPa ($p<0.05$), compared to 3% and 4% Cs-based hydrogels, with an average value

523 of 50 MPa.

524   In order to further study the influence of Cs concentration on the resulting hydrogels

525 structure, their rheological behavior was investigated. The shear (G') and loss (G") moduli

526 curves of the Cs-based hydrogels as a function of strain were considered in the rheometer

527 dynamic stress environment (**Fig. 6B**).

22

528   Profiles displayed that G' values of Cs-based hydrogels increased with the increase of Cs

529 concentration, with an increasing strain from 0.1% to 1000%. In fact, G' of Cs 1%-based

530 hydrogel (15.9 10^3 Pa) at 100% strain was 11.3 times lower than that of Cs 4%-based hydrogel

531 (181 10^3 Pa). Although, in all cases, the storage modulus G' was below the loss modulus G",

532 indicating a predominantly gel-like behavior, the storage modulus G' decreased significantly

533 (p<0.05), reaching 63.2 10^3 Pa, for higher concentration of Cs (5%). In another aspect, 1% Cs-

534 based hydrogel was found to be able to support only around 123% deformation and maintain

535 the gel-like behavior (the point at which G"> G'), while 3% and 4% Cs-based hydrogels were

536 capable to bear more than 574% and 491% deformation, respectively. However, at higher Cs

537 content, le gel structure was kept only at strains below 185% (**Fig. 6B**).

538   Consequently, from the mechanical and rheological testing data, 3% Cs-based hydrogel

539 exhibited better rheological properties than those of 2% Cs, and the fracture deformation was

540 greater than that of 5% Cs. Similarly, excessive Cs concentration led to thicker and too rigid

541 hydrogel, which could be attributed to chains entanglements excess, leading to hydrogels

542 brittleness [61]. However, due to the gradually improved number of the hydrogen-bonded

543 crosslink regions between the Cs chains, in a relatively concentrated solution, aggregation and

544 entanglement amongst the Cs macromolecular chains will significantly took place.

545   Therefore, 3% concentration of chitosan solution was carefully chosen to elaborate Cs-

546 based hydrogels in the following section, for the Riboflavin *in vitro* release study.

547 **3.9. Encapsulation of riboflavin, *in vitro* loading and release profiles**

548   Hydrogels structure is characterized by three major parameters, namely the volume

549 fraction of polymer in the inflated state, the average molecular weight of based polymers as

550 well as the pore size distribution of the network [9-10]. This architecture of hydrogels allows

551 the diffusion of molecules of different sizes in the network, which makes these biomaterials

552 interesting for drug release applications [7,12].

23

553 As the model drug, the kinetics of riboflavin release, through the Cs-based hydrogels were

554 monitored based on the cumulative amounts of released riboflavin as a function of time.

555 Different concentrations of riboflavin (1-5 g/l) were used to investigate the influence of drug

556 concentration on EE and release profiles.

557 The EE and LC of Cs-hydrogels for riboflavin, as reported in **Table 3**, were found to be

558 drug concentration-dependent ($p<0.05$). Indeed, the EE values increased from more than 75%

559 for 1 g/l of riboflavin to about 85% for 3 g/l of riboflavin. However, above 3 g/l of riboflavin,

560 the EE dropped dramatically to 68% and 56%, for 4 g/l and 5 g/l of riboflavin, respectively.

561 Regarding the LC of riboflavin, values increased concomitantly with the increase of drug

562 concentration from 24% for 1 g/l of riboflavin to the saturated capacity of 37% at 3 g/l of

563 riboflavin ($p<0.05$). No significant differences in the riboflavin LC values was noted beyond 3

564 g/l of riboflavin ($p\geq0.05$). The decrease in the amount of encapsulated riboflavin at high

565 concentration could be related to the saturation of hydrogel (limitation of riboflavin loading

566 into Cs-based hydrogel), since the encapsulation of riboflavin was monitored through its

567 diffusion in the hydrogel network.

568 Riboflavin release profiles from Cs-based hydrogels, at 37 °C, in HCl-NaOH (0.1 M), pH

569 5.5, exhibited deliverance patterns, characterized by an initial short-time rapid release, during

570 the first 8 h, followed by low riboflavin release to 72 h. Beyond 72 h, the rate of released

571 riboflavin tended to stabilize (**Fig. 7**). Data reveal that hydrogel with lower riboflavin charge

572 showed high initial release in terms of percentage. Indeed, at a riboflavin concentration of 1 g/l,

573 the initial release rate (after 4 h) was 11% relative to the amount of initial riboflavin loaded in

574 the hydrogel. It was of 46% and 79%, after 24 h and at the end of the study (96 h). Regarding

575 a concentration of 5 g/l, the release of riboflavin was 5%, 18% and 36%, after 4 h, 24 h and 96

576 h, respectively. In terms of the total mass of riboflavin released, the hydrogel group with higher

577 charge released more riboflavin. For example, at a riboflavin concentration of 1 g/l, the amount

24

578 released riboflavin was 790 mg after 96 h, while for the 5 g/l riboflavin hydrogel group, about

579 2 g of riboflavin were released (**Fig. 7A**). This finding could be assigned to the concentration

580 gradient phenomenon as diffusion management force. The more Riboflavin loading increased,

581 the higher concentration gradient increased [27].

582   The riboflavin (3 g/l) release patterns were further investigated in HCl-NaCl (0.1 M)

583 under different pH conditions (pH 2.0, pH 4.5 and pH 7.4). Deliverance curves, as reported in

584 **Fig. 7B**, showed that riboflavin was barely released from the Cs-based hydrogels, at pH 7.4, of

585 only 13% after 4 days of incubation. However, high amounts of riboflavin were released in

586 acidic pH (p<0.05), further, the amount of released riboflavin from Cs-based hydrogels was

587 higher in pH than pH 4.5 in pH 2.0. Indeed, 16% and 38% of riboflavin were released from Cs-

588 based hydrogel, after 8 h, at pH 4.5 and pH 2.0, respectively. Therefore, Cs-hydrogels were

589 found to release significantly more riboflavin in acidic microenvironments, probably due to

590 higher swelling rates or exhaustive hydrogels structure destruction and thereby faster

591 degradation and release of riboflavin [26,59,60].

592 **4. Conclusion**

593   Different Cs-based hydrogels were successfully engineered, considering Cs AD and Mw,

594 based on the alkali/urea aqueous system following the freezing/thawing/solvent evaporation

595 approach. As expected, hydrogels pore size distribution, mechanical strength, swelling and

596 thermal resistance behaviors besides the *in vitro* biodegradation patterns, were extremely

597 depending on Cs structural characteristics. Low AD coupled with high Mw seemed to be very

598 interesting for the development of promoting biomaterials with stable and appropriate features.

599   Moreover, Cs-based hydrogels were monitored to study the *in vitro* release of riboflavin

600 selected as the model drug. The obtained release patterns displayed that Cs-based hydrogels

601 could be applied as smart pH-sensitive carrier for drug-controlled release for further biomedical

602 applications (antitumor, protein and peptide, gene and antibiotic drug delivery). Additionally,

25

due to its suitable structural architecture, swelling behavior and mechanical strength, the application of Cs-based hydrogels seems to be a very interesting alternative in the tissue engineering field.

Acknowledgement

References

1. B. Tavsanli, O. Okay. Mechanically Robust and Stretchable Silk/hyaluronic Acid Hydrogels. *Carbohydr. Polym* 2019, 208, 413-420.
2. M. Khan, J.T. Koivisto, T.I. Hukka, M. Hokka, M. Kellomäki. Composite Hydrogels Using Bioinspired Approach With In Situ Fast Gelation and Self-healing Ability as Future Injectable Biomaterial. *ACS Appl. Mater. Interfaces* 2018, 10, 11950-11960.
3. N. Martin, G. Youssef. Dynamic Properties of Hydrogels and Fiber-reinforced Hydrogels. *J. Mech. Behav. Biomed. Mater* 2018, 85, 194-200.
4. S. Ma, B. Yu, X. Pei, F. Zhou. Structural Hydrogels. *Polymer* 2016, 98, 516-535.
5. J. Duan, X. Liang, Y. Cao, Se. Wang, Zhang, L. High Strength Chitosan Hydrogels with Biocompatibility via New Avenue Based on Constructing Nanofibrous Architecture. *Macromolecules* 2015, 48, 2706-2714.
6. W. Wang, Y. Zhao, H. Yi, T. Chen, S. Kang, T. Zhang, F. Rao, S. Song. Pb(II) Removal from Water Using Porous Hydrogel of Chitosan-2D Montmorillonite. *Int. J. Biol. Macromol* 2019, 128, 85-93.
7. L. Liu, Q. Gao, X. Lu, H. Zhou. In Situ Forming Hydrogels Based on Chitosan for Drug Delivery and Tissue Regeneration. *Asian J. Pharm. Sci* 2016, 11, 673–683.
8. Y.H. Cheng, Y.C. Ko, Y.F. Chang, S.H. Huang, C.J.L. Liu. Thermosensitive Chitosan-gelatin-based Hydrogel Containing Curcumin-loaded Nanoparticles and Latanoprost as a Dual-drug Delivery System for Glaucoma Treatment. *Exp. Eye Res* 2019, 179, 179-187.
9. R. Dimatteo, N.J. Darling, T. Segura. In Situ Forming Injectable Hydrogels for Drug Delivery and Wound Repair. *Adv. Drug Deliv. Rev* 2018, 127, 167–184.
10. T.M. Aminabhavi, S.P. Dharupaneedi. Production of Chitosan-based Hydrogels for Biomedical Applications. *Chitosan Based Biomaterials Volume 1 – Fundamentals* 2017, 295-319.
11. A.M. Slavutsky, M.A. Bertuzzi, Formulation and Characterization of Hydrogel Based on Pectin and Brea Gum. *Int. J. Biol. Macromol* 2019, 123, 784-791.
12. Z. Huang, C. Gao, Y. Huang, X. Zhang, X. Deng, Q. Cai. Injectable polyphosphazene/gelatin hybrid hydrogel for biomedical applications. *Mater. Des* 2008, 160, 1137–1147.

26

13. Annu, K. Manzoor, S. Ahmad, A. Soundarajan, S. Ikram, S. Ahmed. Chitosan Based Nanomaterials for Biomedical Applications. *Handbook of Nanomaterials for Industrial Applications, Micro and Nano Technologies* 2018, 543-562.

14. B. Choi, S. Kim, B. Lin, B.M. Wu, M. Lee. Cartilaginous Extracellular Matrix-Modified Chitosan Hydrogels for Cartilage Tissue Engineering. *ACS Appl. Mater. Interfaces* 2014, 6, 20110−20121.

15. E. Calo, V.V. Khutoryanskiy. Biomedical Applications of Hydrogels: A Review of Patents and Commercial Products. *Eur. Polym. J* 2015, 65, 252-267.

16. G. Camci-Unal, P. Zorlutuna, A. Khademhosseini. Chapter 4 - Fabrication of Microscale Hydrogels for Tissue Engineering Applications. *Biofabrication, Micro- and Nano-fabrication, Printing, Patterning and Assemblies* 2013, 59-80.

17. S.Z. Md Rasib, H. Md Akil, A. Khan, Z.A.A. Hamid. Controlled Release Studies Through Chitosan-based Hydrogel Synthesized at Different Polymerization Stages. *Int. J. Biol. Macromol* 2019, 128, 531-536.

18. F.A. Fookes, L.N. Mengatto, A. Rigalli, J.A. Luna. Controlled Fluoride Release for Osteoporosis Treatment Using Orally Administered Chitosan Hydrogels. *J. Drug Deliv. Sci. Technol* 2019, 51, 268-275.

19. B. Onat, S. Ulusan, S. Banerjee, E. Erel-Goktepe. Multifunctional Layer-by-layer Modified Chitosan/poly(Ethylene Glycol) Hydrogels. *Eur. Polym. J* 2019, 112, 73-86.

20. K. Saekhor, W. Udomsinprasert, S. Honsawek, W. Tachaboonyakiat. Preparation of an Injectable Modified Chitosan-based Hydrogel Approaching for Bone Tissue Engineering. *Int. J. Biol. Macromol* 2019, 123, 167-173.

21. M. Hamdi, S. Hajji, S. Affes, W. Taktak, H. Maâlej, M. Nasri, R. Nasri. Development of a Controlled Bioconversion Process for The Recovery of Chitosan from Blue Crab (*Portunus segnis*) Exoskeleton. *Food Hydrocoll* 2018, 77, 534-548.

22. S.H. Chang, H.T.V. Lin, G.J. Wu, G.J. Tsai. pH Effects on Solubility, Zeta Potential, And Correlation Between Antibacterial Activity and Molecular Weight of Chitosan. *Carbohydr. Polym* 2015, 134, 74-81.

23. R.Q. Qian, R.W. Glanville. Methods for Purifying Chitosan. *US Patent* 2005, 6896809.

24. B. Huang, M. Liu, C. Zhou. Chitosan Composite Hydrogels Reinforced with Natural Clay Nanotubes. *Carbohydr. Polym* 2017, 175, 689-698.

25. AOAC. Official Methods of Analysis (17th ed.). Washington, DC: *Association of Official Analytical Chemists* 2000.

26. S. Yu, X. Zhang, G. Tan, L. Tian, D. Liu, Y. Liu, X. Yang, W. Pan. A Novel pH-Induced Thermosensitive Hydrogel Composed of Carboxymethyl Chitosan and Poloxamer Cross-Linked by Glutaraldehyde for Ophthalmic Drug Delivery. *Carbohydr. Polym* 2017, 155, 208–217.

27. J. Qu, X. Zhao, P.X. Ma, B. Guo. pH-Responsive Self-Healing Injectable Hydrogel Based On N-Carboxyethyl Chitosan for Hepatocellular Carcinoma Therapy. *Acta Biomater* 2017, 58, 168-180.

28. B. Wang, B. Adhikari, C.J. Barrow. Highly Stable Spray Dried Tuna Oil Powders Encapsulated in Double Shells of Whey Protein Isolate-Agar Gum and Gellan Gum Complex Coacervates. *Powder Technol* 2018, In Press, Corrected Proof.

29. H. Ge, T. Hua, J. Wang. Preparation and Characterization of Poly (Itaconic Acid)-Grafted Crosslinked Chitosan Nanoadsorbent For High Uptake of Hg2+ And Pb2+. *Int. J. Biol. Macromol* 2017, 95, 954-961.

30. A.M. Heimbuck, T.R. Priddy-Arrington, B.J. Sawyer, M.E. Caldorera-Moore. Effects of Post-Processing Methods on Chitosan-Genipin Hydrogel Properties. *Mater. Sci. Eng. C* 2019, 98, 612–618.

31. M.C.G. Pella, M.K. Lima-Tenorio, E.T. Tenorio-Neto, M.R. Guilherme, E.C. Muniz, A.F. Rubira. Chitosan-Based Hydrogels: From Preparation to Biomedical Applications. *Carbohydr. Polym* 2018, 196, 233-245.

32. M.L. Tsai, H.W. Chang, H.C. Yu, Y.S. Lin, Y.D. Tsai. Effect of Chitosan Characteristics and Solution Conditions on Gelation Temperatures of Chitosan/2-Glycerophosphate/Nanosilver Hydrogels. *Carbohydr. Polym* 2011, 84, 1337-1343.

33. F. Wang, Y. Wen, T. Bai. The Composite Hydrogels of Polyvinyl Alcohol–Gellan Gum Ca2+ With Improved Network Structure and Mechanical Property. *Mater. Sci. Eng. C* 2016, 69, 268–275.

34. B. Ding, H. Gao, J. Song, Y. Li, L. Zhang, X. Cao, M. Xu, J. Cai. Tough and Cell-Compatible Chitosan Physical Hydrogels for Mouse Bone Mesenchymal Stem Cells *in Vitro*. *ACS Appl. Mater. Interfaces* 2016, 10, 19739-19746.

35. Y. Yao, M. Xia, H. Wang, G. Li, H. Shen, G. Ji, Q. Meng, Y. Xie. Preparation and Evaluation of Chitosan-Based Nanogels/Gels for Oral Delivery of Myricetin. *Eur. J. Pharm. Sci* 2016, 91, 144-153.

36. L. Zhang, Y. Li, L. Li, B. Guo, P.X. Ma. Non-Cytotoxic Conductive Carboxymethyl-Chitosan/Aniline Pentamer Hydrogels. *React. Funct. Polym* 2014, 82, 81-88.

37. X. Zhao, P. Li, B. Guo, P.X. Ma. Antibacterial and Conductive Injectable Hydrogels Based on Quaternized Chitosan-Graft-Polyaniline/Oxidized Dextran for Tissue Engineering. *Acta Biomater* 2015, 26, 236-248.

38. C. Chang, S. Chen, L. Zhang. Novel Hydrogels Prepared Via Direct Dissolution of Chitin at Low Temperature: Structure and Biocompatibility. *J. Mater. Chem* 2011, 21, 3865-3872.

39. E. Assaad, M. Maire, S. Lerouge. Injectable Thermosensitive Chitosan Hydrogels with Controlled Gelation Kinetics and Enhanced Mechanical Resistance. *Carbohydr. Polym* 2015, 130, 87–96.

40. Q. Wang, S. Chen, D. Chen. Preparation and Characterization of Chitosan Based Injectable Hydrogels Enhanced by Chitin Nano-Whiskers. *J. Mech. Behav. Biomed. Mater* 2017, 65, 466–477.

41. M. Fan, Q. Hu. Superadsorption Of LiOH Solution on Chitosan as A New Type of Solvent for Chitosan by Freezing/Blasting. *Carbohydr. Polym* 2013, 94, 430– 435.

42. L. Cui, J. Jia, Y. Guo, Y. Liu, P. Zhu. Preparation and Characterization of IPN Hydrogels Composed of Chitosan and Gelatin Cross-Linked by Genipin. *Carbohydr. Polym* 2014, 99, 31-38.

43. X.J. Liu, Y. Chen, Q.L. Huang, W. He, Q.L. Feng, B. Yu. A Novel Thermo-Sensitive Hydrogel Based on Thiolated Chitosan/Hydroxyapatite/Beta-Glycerophosphate. *Carbohydr. Polym* 2014,110, 62-9.

44. Y. Ogawa, S. Kimura, M. Wada, S. Kuga. Crystal analysis and high-resolution imaging of microfibrillar α-chitin from Phaeocystis. *J. Struct. Biol* 2010, 171, 111–116.

28

45. N. Vasanthan, I.D. Shin, A.E. Tonelli. Structure, Conformation, And Motions Of Poly(Ethylene Oxide) And Poly(Ethylene Glycol) In Their Urea Inclusion Compounds. *Macromolecules* 1996, 29, 263–267.

46. A.L. Skwarczynska, D. Binias, W. Maniukiewicz, Z. Modrzejewska, T.E.L. Douglas. The Mineralization Effect on Chitosan Hydrogel Structure Containing Collagen and Alkaline Phosphatase. *J. Mol. Struct* 2019, 1187, 86-97.

47. Y. Liu, Z. Liu, W. Pan, Q. Wu. Absorption Behaviors and Structure Changes of Chitin in Alkali Solution. *Carbohydr. Polym* 2008, 72, 235–239.

48. X. Liang, J. Duan, Q. Xu, X. Wei, A. Lu, L. Zhang. Ampholytic Microspheres Constructed from Chitosan and Carrageenan in Alkali/Urea Aqueous Solution for Purification of Various Wastewater. *Chem. Eng. J* 2017, 317, 766-776.

49. H.Y. Zhou, L.J. Jiang, P.P. Cao, J.B. Li, X.G. Chen. Glycerophosphate-Based Chitosan Thermosensitive Hydrogels and Their Biomedical Applications. *Carbohydr. Polym* 2015, 117, 524-53.

50. M.R. Saboktakin, R.M. Tabatabaie, A. Maharramov, M.L. Ramazanov. Synthesis And In Vitro Studies of Biodegradable Thiolated Chitosan Hydrogels for Breast Cancer Therapy. *Int. J. Biol. Macromol* 2011, 48, 747-752.

51. Y. Xie, X. Liao, J. Zhang, F. Yang, Z. Fan. Novel Chitosan Hydrogels Reinforced by Silver Nanoparticles with Ultrahigh Mechanical and High Antibacterial Properties for Accelerating Wound Healing. *Int. J. Biol. Macromol* 2018, 119, 402-412.

52. M.A. Gamiz-González, D.M. Correia, S. Lanceros-Mendez, V. Sencadas, J.L. Gómez Ribelles, A. Vidaurre. Kinetic Study of Thermal Degradation of Chitosan as A Function of Deacetylation Degree. *Carbohydr. Polym* 2017, 167, 52-58.

53. Z. Bao, C. Jiang, Z. Wang, Q. Ji, G. Sun, S. Bi, Y. Liu, X. Chen. The Influence of Solvent Formulations on Thermosensitive Hydroxybutyl Chitosan Hydrogel as A Potential Delivery Matrix for Cell Therapy. *Carbohydr. Polym* 2017, 170, 80-88.

54. J. Maity, S.K. Ray. Removal of Cu (II) Ion from Water Using Sugar Cane Bagasse Cellulose and Gelatin Based Composite Hydrogels. *Int. J. Biol. Macromol* 2016, 97, 238-248.

55. S. Bi, Z. Bao, X. Bai, S. Hu, X. Cheng, X. Chen. Tough Chitosan Hydrogel Based on Purified Regeneration and Alkaline Solvent as Biomaterials for Tissue Engineering Applications. *Int. J. Biol. Macromol* 2017, 104, 224-231.

56. F. Wahid, X.H. Hu, L.Q. Chu, S.R. Jia, Y.Y. Xie, C. Zhong. Development of Bacterial Cellulose/Chitosan Based Semi-Interpenetrating Hydrogels with Improved Mechanical and Antibacterial Properties. *Int. J. Biol. Macromol* 2019, 122, 380-387.

57. Z. Naghizadeh, A. Karkhaneh, A. Khojasteh. Self-Crosslinking Effect of Chitosan and Gelatin on Alginate-Based Hydrogels: Injectable in Situ Forming Scaffolds. *Mater. Sci. Eng. C* 2018, 89, 256-264.

58. C. Chang, M. He, J. Zhou, L. Zhang. Swelling Behaviors of pH- and Salt-Responsive Cellulose-Based Hydrogels. *Macromolecules* 2011, 44, 1642–1648.

59. S. Zang, R. Mu, F. Chen, X. Wei, L. Zhu, B. Han, H. Yu, B. Bi, B. Chen, Q. Wang, L. Jin. Injectable Chitosan/B-Glycerophosphate Hydrogels with Sustained Release Of BMP-7 And Ornidazole In Periodontal Wound Healing of Class III Furcation Defects. *Mater. Sci. Eng. C* 2019, 99, 919-928.

29

770 60. Y. Ren, X. Zhao, X. Liang, P.X. Ma, B. Guo. Injectable Hydrogel Based on Quaternized
771   Chitosan, Gelatin and Dopamine as Localized Drug Delivery System to Treat Parkinson's
772   Disease. *Int. J. Biol. Macromol* 2017, 105, 1079-1087.
773 61. D. Zhao, J. Huang, Y. Zhong, K. Li, L. Zhang, J. Cai. High-Strength and High-Toughness
774   Double-Cross-Linked Cellulose Hydrogels: A New Strategy Using Sequential Chemical and
775   Physical Cross-Linking. *Adv. Funct. Mater* 2016, 26, 1-9.

Figure 1: SEM images of Cs-based hydrogels (GCs) cross sections: GCsI-0 with AD of 17% and Mw of 125.6 kDa **(A)**, GCsI-1 with AD of 17% and Mw of 17.8 kDa, **(B)** GCsI-3 with AD of 17% and Mw of 10.44 kDa **(C)**, GCsII-0 with AD of 13% and Mw of 118.9 kDa **(D)**, GCsII-1 with AD of 13% and Mw of 59.27 kDa **(E)**, GCsII-3 with AD of 13% and Mw of 18.54 kDa **(F)**, GCsIII-0 with AD of 8% and Mw of 115 kDa **(G)**, GCsIII-1 with AD of 8% and Mw of 78.43 kDa **(H)** and GCsIII-3 with AD of 8% and Mw of 16.04 kDa **(I)**.

Figure 2: ATR-FTIR profiles of Cs-based hydrogels (GCs) with different AD and Mw, **(A)** GCsI, **(B)** GCsII and **(C)** GCsIII, compared to Cs powders spectra.

Figure 3: XRD patterns of Cs-based hydrogels (GCs) with different AD and Mw, **(A)** GCsI, **(B)** GCsII and **(C)** GCsIII, compared to Cs powders spectra.

Figure 4: Mechanical features of Cs-based hydrogels (GCs) as function of Cs AD and Mw. Rheological behavior **(A)** GCsI, **(B)** GCsII, **(C)** GCsIII, f=1 Hz, T=37 °C. Compressive properties, at a temperature of 25 °C and a compression speed of 1 mm/min, **(D)** GCsI, **(E)** GCsII, **(F)** GCsIII.

Figure 5: *In vitro* biodegradation Cs-based hydrogels (GCs) as function of Cs AD and Mw, in PBS at **(A)** pH 5.5 (acidic microenvironment) and **(B)** pH 7.4 (physiological microenvironment simulation), at 37 °C.

Figure 6: Mechanical behavior of Cs-based hydrogels as function of Cs concentration. **(A)** Compressive stress vs. compressive strain profiles. **(B)** Viscoelastic properties patterns as function of strain (%), f=1 Hz, T=37 °C.

Figure 7: Riboflavin, as the model drug, *in vitro* release profile and kinetics from Cs-based hydrogels. Riboflavin incorporation was monitored by immersion in riboflavin solution (0-5 g/l) in dark at 5 °C for 48 h. The release tests were performed in HCl and NaCl (0.1 M) with different pH values (pH 2.0, pH 4.5 and pH 7.4) at 37 °C. **(A)** Riboflavin release kinetics at different concentrations (0-5 g/l of riboflavin) in pH 5.5. **(B)** Riboflavin (3 g/l) release kinetics at different pH values (pH 2.0, pH 4.5 and pH 7.4).
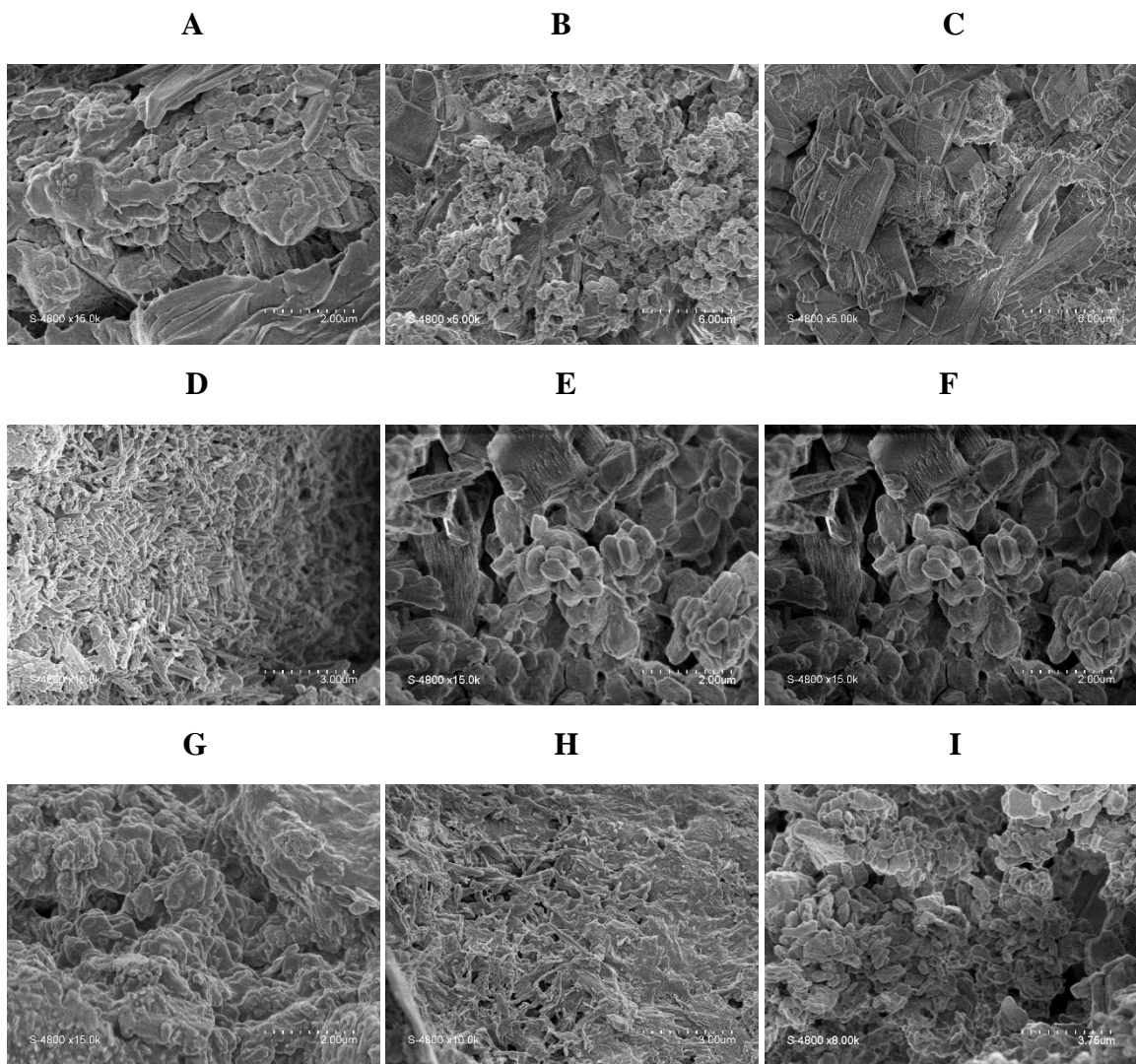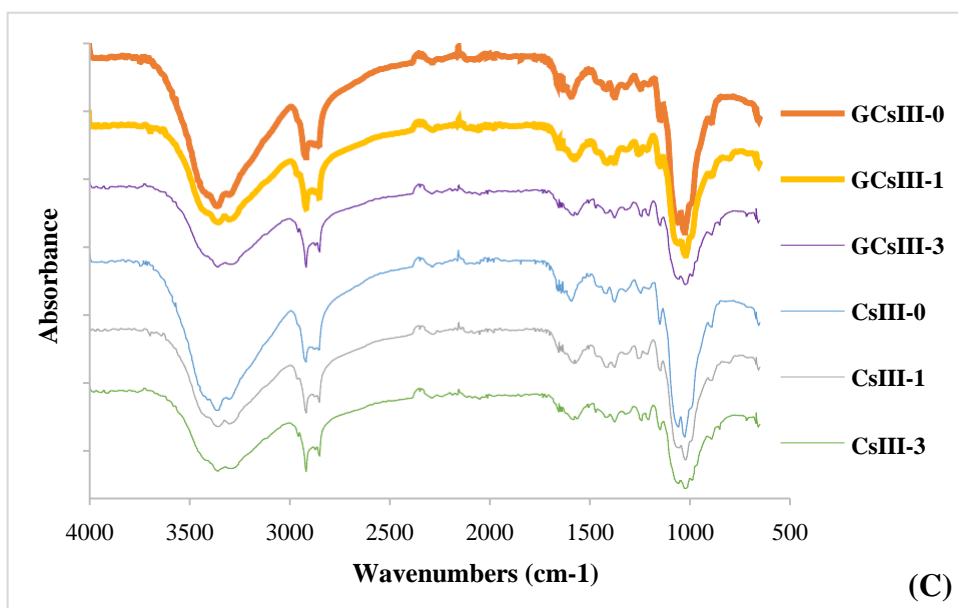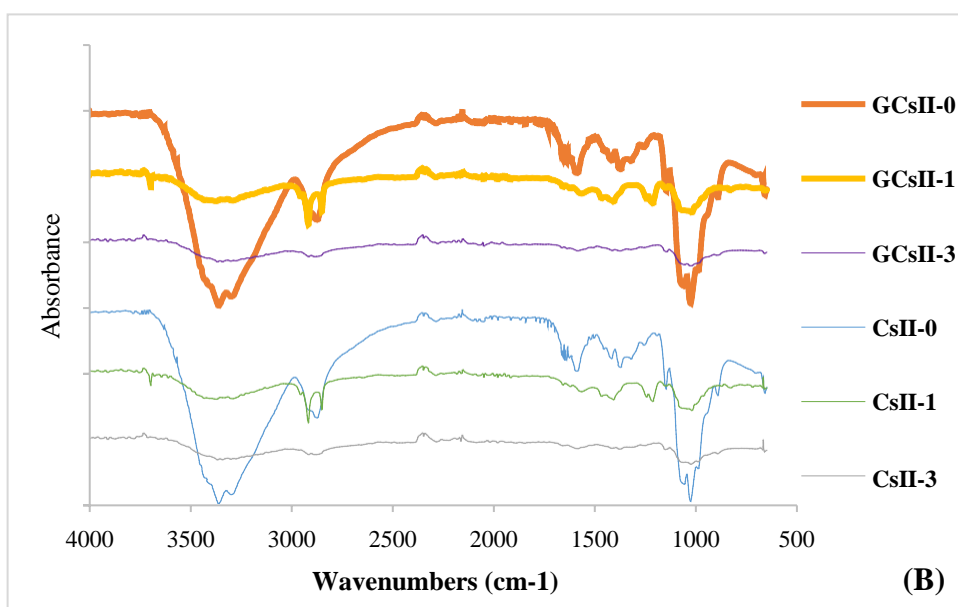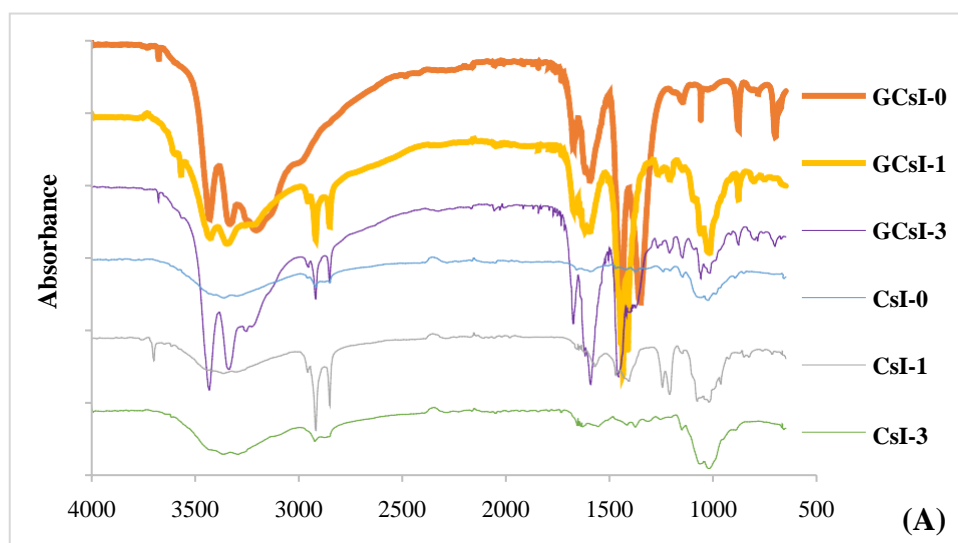
Fig. 1

Fig. 2

(A)

(B)

Wavenumbers (cm-1)

(C)

Wavenumbers (cm-1)

Fig. 3
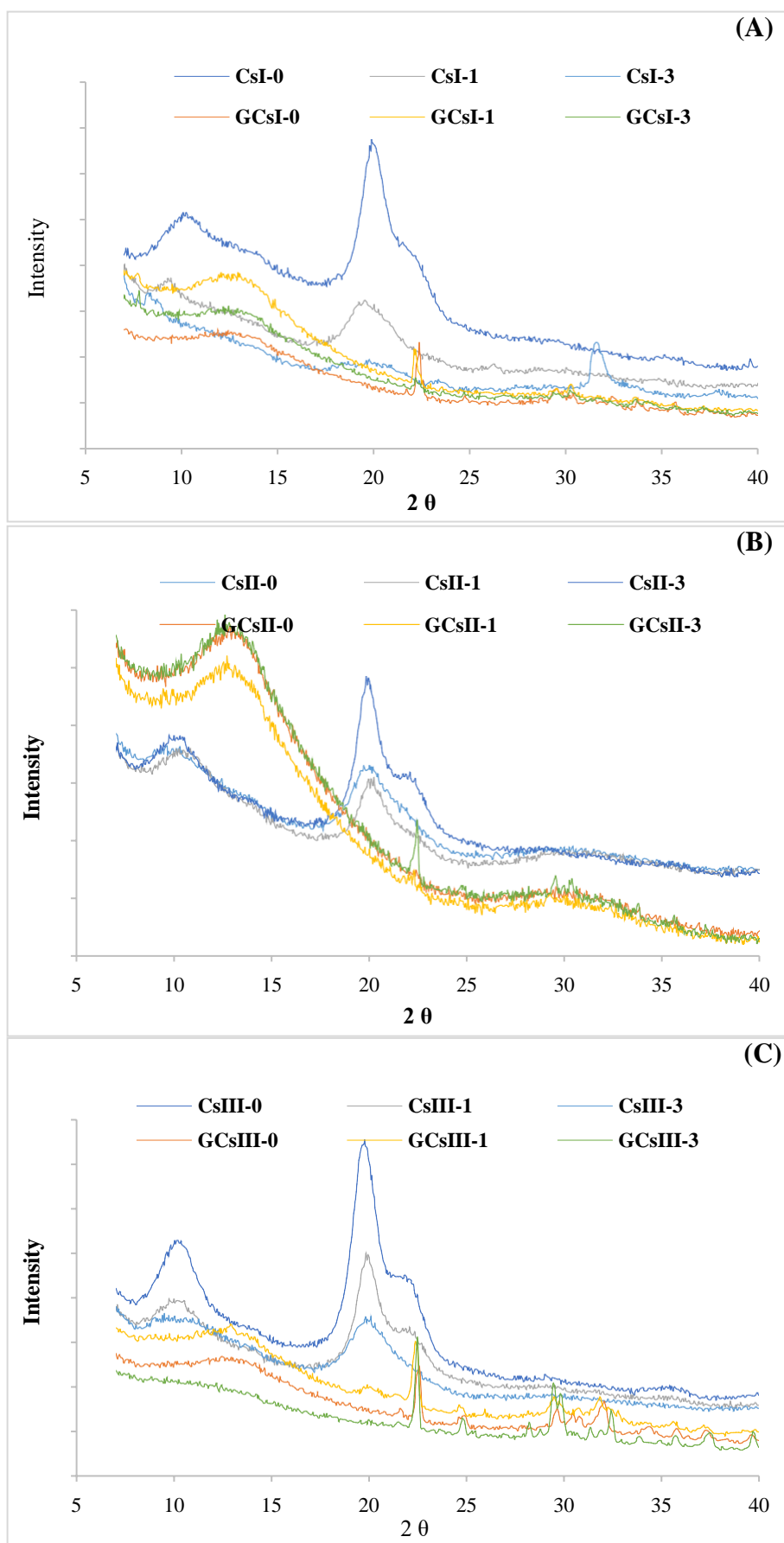
Fig. 4
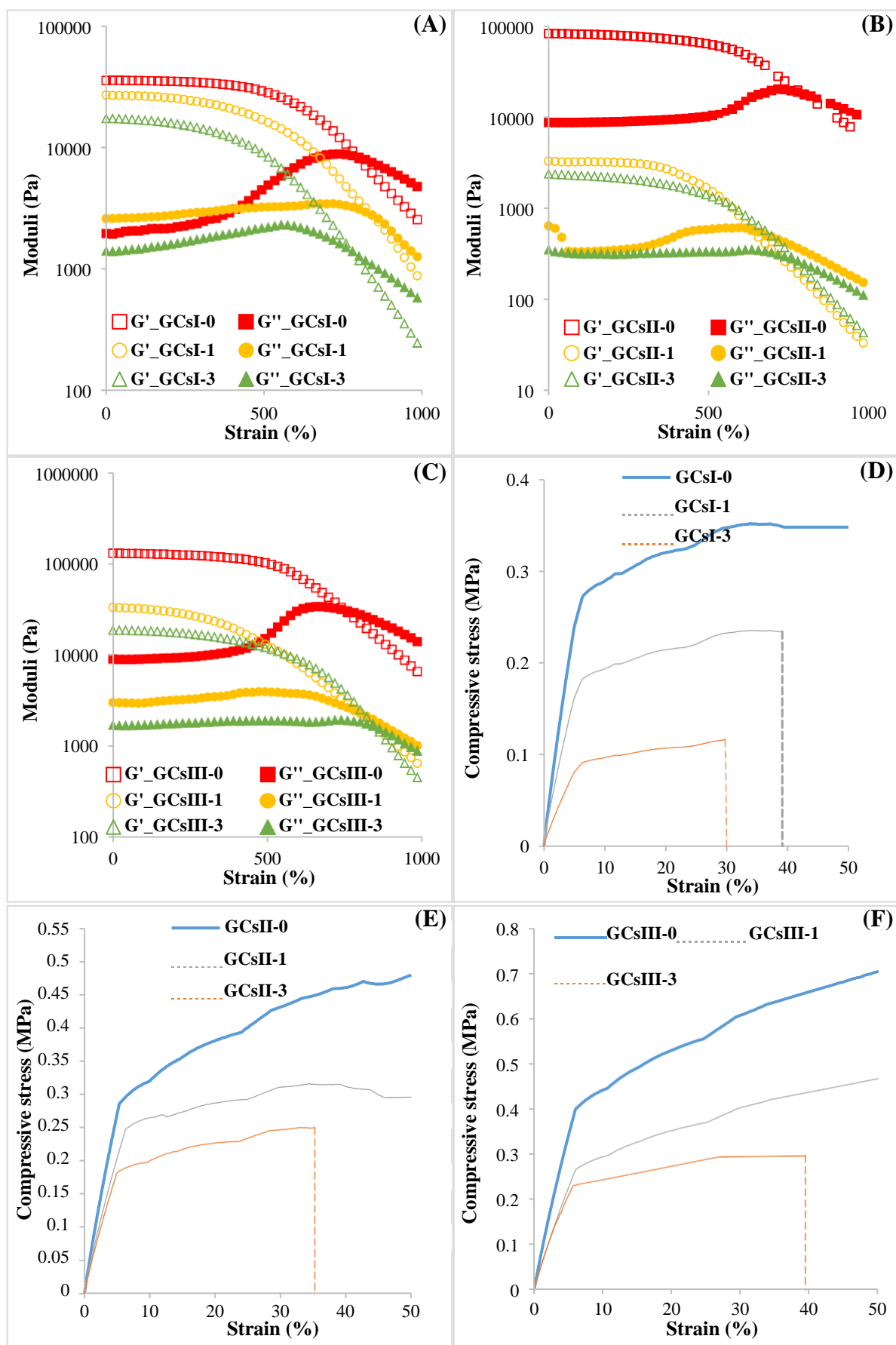
Fig. 5
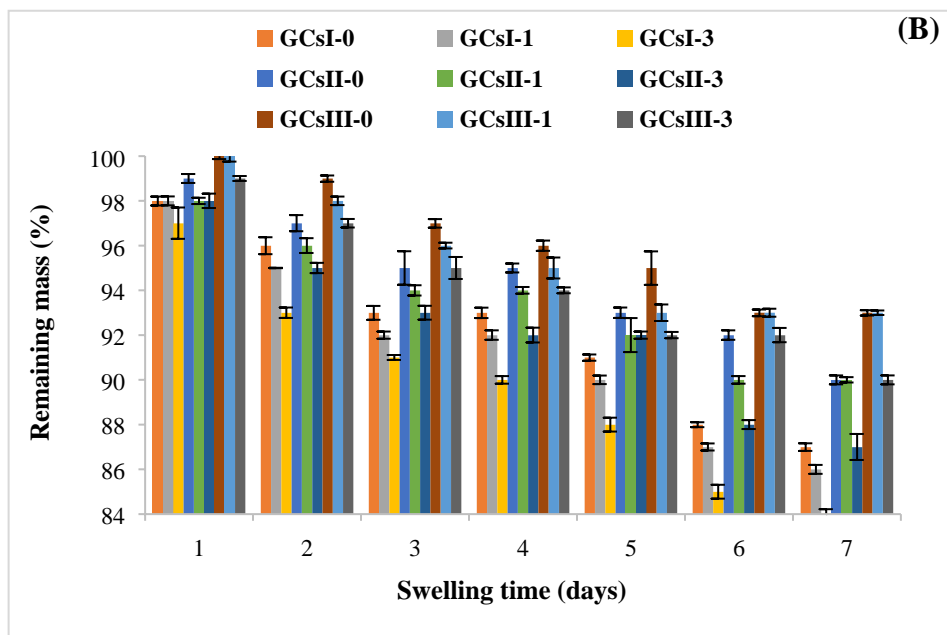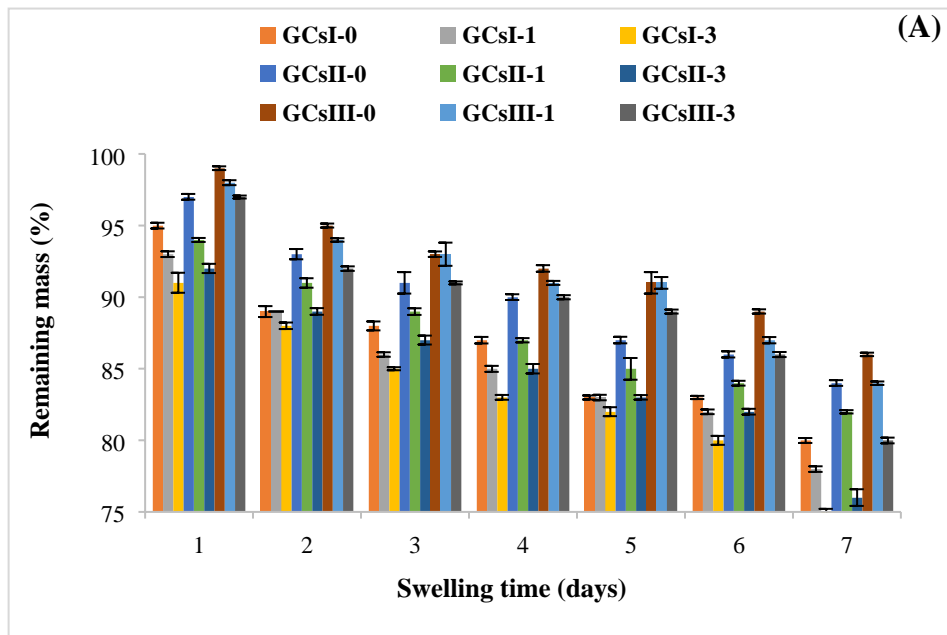
Fig. 6
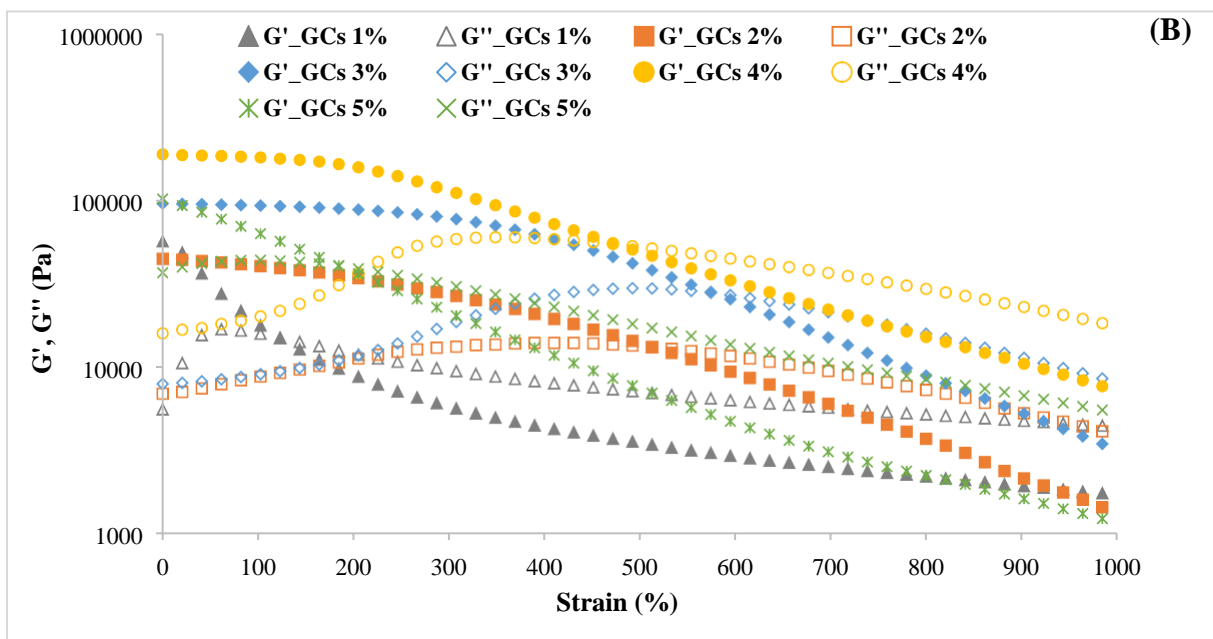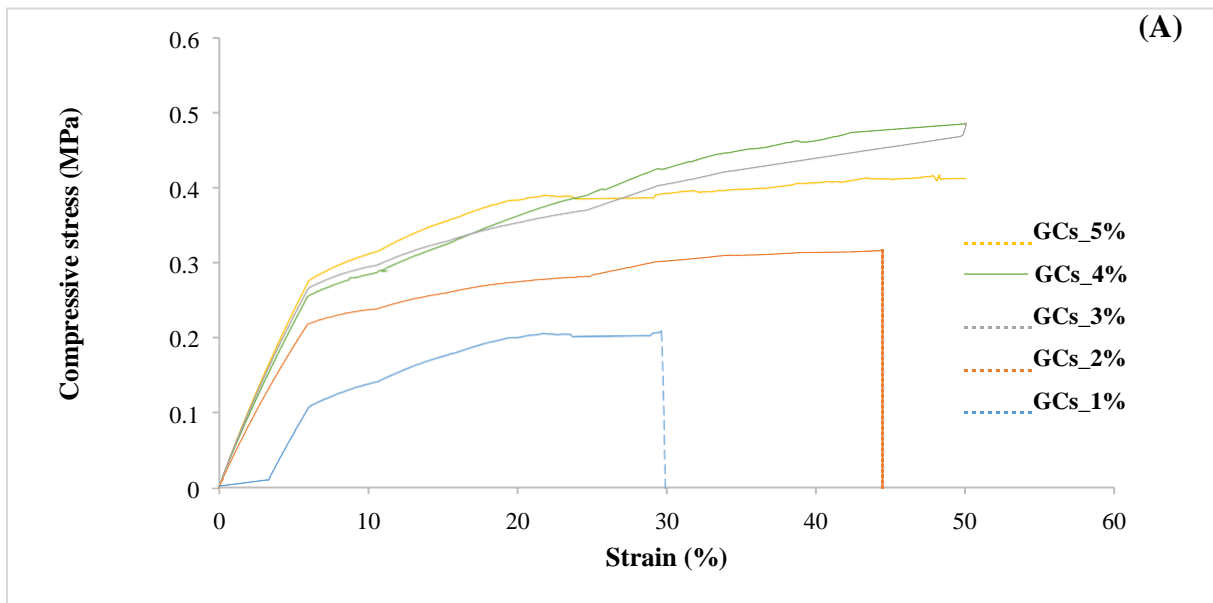
Fig. 7

Fig. S1

Fig. S2
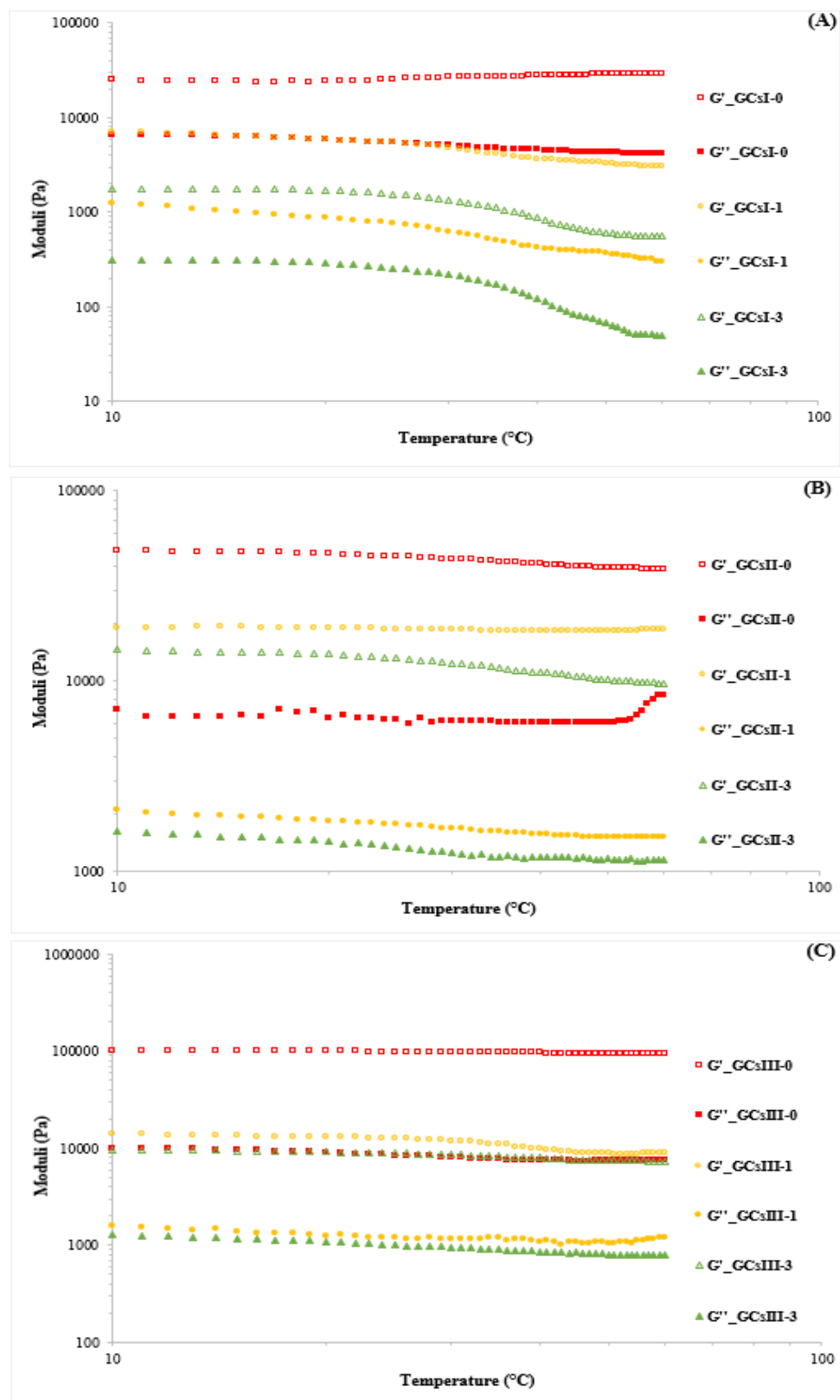
Table 1: Moisture content (MC) and swelling ratio (SR) of different prepared Cs-based

hydrogels.

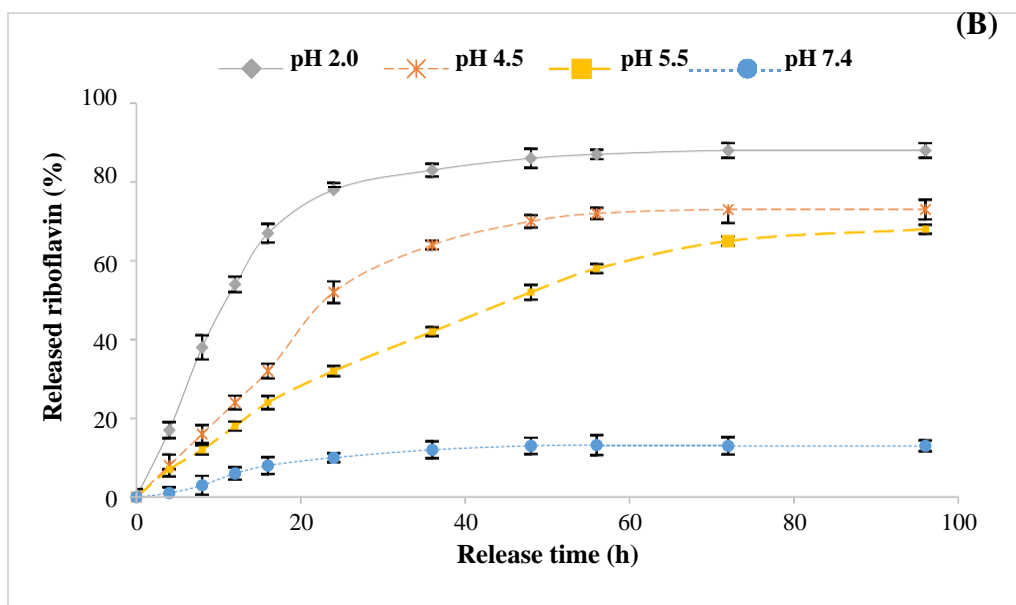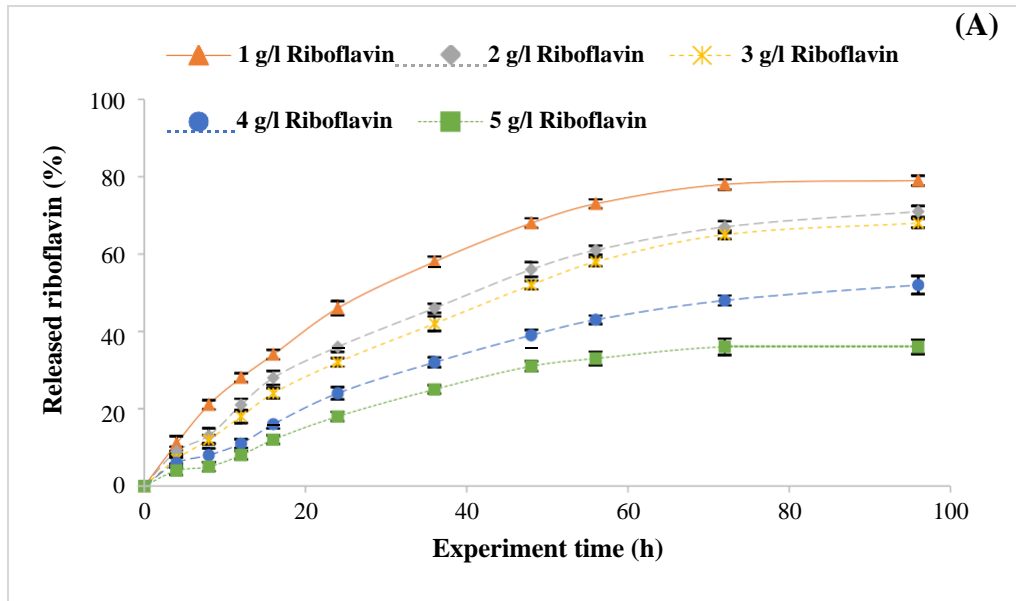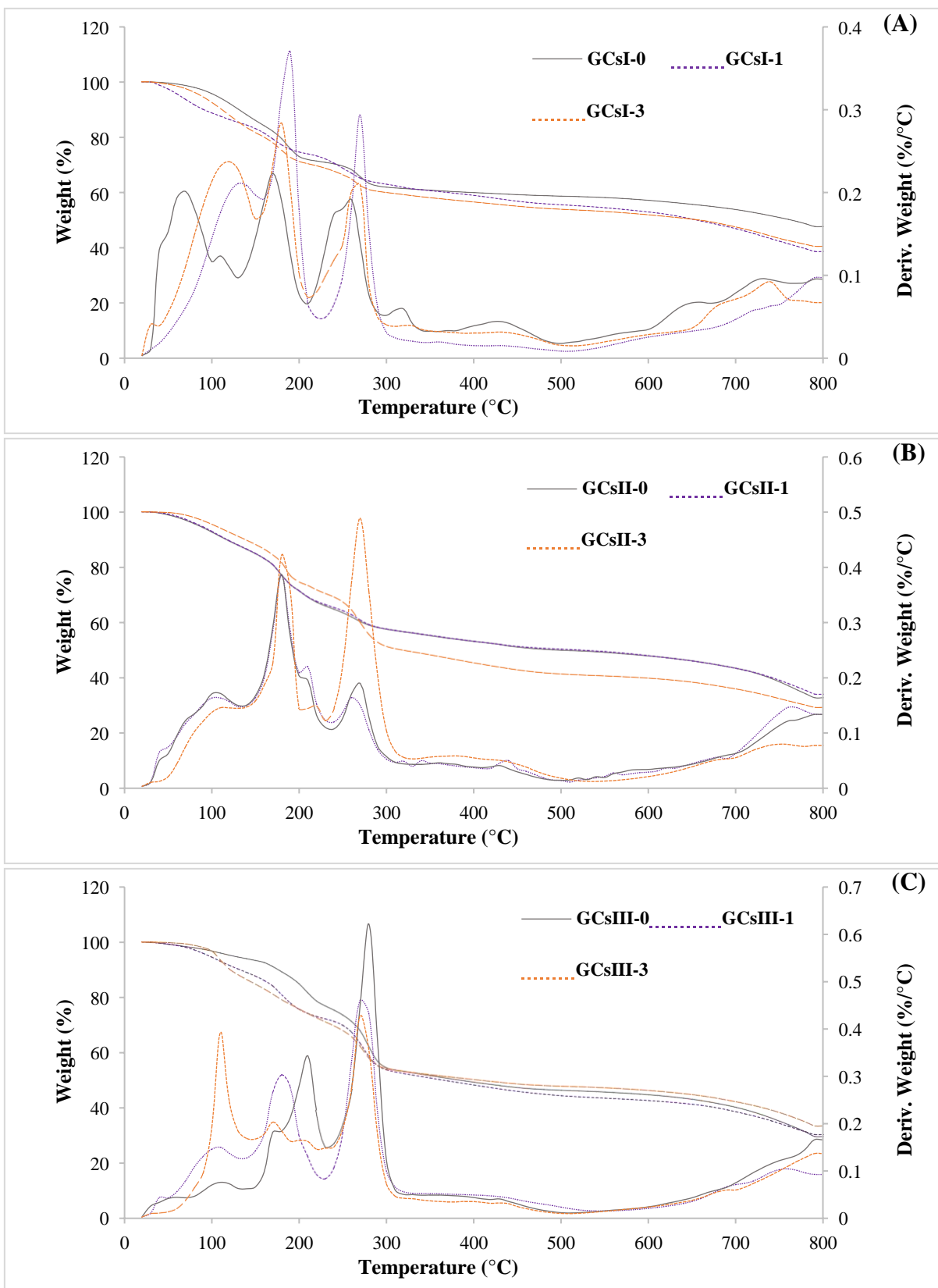| Cs-based hydrogels	3% (w/v) Cs content					
	GCsI		GCsII		GCsIII	
	MC (%)	SR (g/g)	MC (%)	SR (g/g)	MC (%)	SR (g/g)
GCs-0	82.36±0.72 [aB]	13.59±0.45 [aA]	81.34±0.22 [aB]	16.57±1.04 [aB]	79.90±0.09 [aA]	18.10±0.47 [aC]
GCs-1	86.52±1.35 [bC]	14.92±0.32 [bA]	81.78±0.11 [aB]	18.93±0.32 [bB]	80.26±0.04 [bA]	22.21±0.53 [bC]
GCs-3	89.08±0.69 [cC]	16.38±0.27 [cA]	83.20±0.06 [bB]	22.86±0.78 [cB]	81.83±0.08 [cA]	26.24±0.93 [cC]

Different letters (a-c) in the same column are significantly different as determined by ANOVA test ($p < 0.05$).

Different letters (A-C) in the same line indicated significant differences within hydrogels based on Cs with different AD ($p < 0.05$).

Table 2: Cs-based hydrogels degradation temperatures (**Td:** onset temperature of degradation, **Tmax:** maximum degradation temperature and **Tf:** temperature of the end of degradation), the weight loss (**Δw**) and the residue (**R**).

Parameters		GCsI			GCsII			GCsIII		
	-	GCsI-0	GCsI-1	GCsI-3	GCsII-0	GCsII-1	GCsII-3	GCsIII-0	GCsIII-1	GCsIII-3
Phase I	ΔW (%)	11.46	15.69	18.93	8.66	12.14	12.73	5.65	10.30	14.75
	Td (°C)	27.32	33.30	40.93	30.03	37.75	42.75	36.39	41.71	45.47
	Tmax (°C)	114.47	104.49	66.35	118.10	109.02	104.49	133.54	109.93	106.35
	Tf (°C)	147.16	133.54	129.00	153.51	134.45	129.91	158.96	135.35	130.81
Phase II	ΔW (%)	13.30	14.43	10.72	20.95	21.24	22.50	17.18	18.19	14.04
	Td (°C)	147.16	133.54	129.00	153.51	134.45	129.91	158.96	135.35	130.81
	Tmax (°C)	184.38	176.21	169.85	188.01	179.84	172.58	208.89	179.84	175.30
	Tf (°C)	227.05	210.71	207.08	235.22	229.77	226.13	235.22	231.59	227.05
Phase III	ΔW (%)	12.42	16.59	18.63	29.34	15.52	15.29	28.77	29.72	23.29
	Td (°C)	227.05	210.71	207.08	235.22	229.77	226.13	235.22	231.59	227.05
	Tmax (°C)	268.81	266.09	261.55	269.72	267.00	262.46	279.71	274.26	273.35
	Tf (°C)	511.22	507.58	502.14	537.54	508.49	502.14	547.53	510.31	509.40
	R (%)	38.68	40.53	47.69	29.58	33.05	34.34	29.88	30.59	33.70

Table 3: Riboflavin entrapment efficiency (EE) and loading capacity (LC) of CsIII-0 based hydrogel, at a concentration of 3% (w/v).

Riboflavin concentration (g/l)	EE (%)	LC (%)
1	75.58 ± 0.61 [c]	23.51 ± 1.26 [a]
2	80.64 ± 1.59 [d]	31.14 ± 0.94 [b]
3	84.54 ± 1.35 [e]	36.57 ± 1.45 [c]
4	66.28 ± 0.52 [b]	37.19 ± 0.62 [c]
5	53.27 ± 1.72 [a]	37.81 ± 1.32 [c]

Different letters (a-e) in the same column are significantly different as determined by ANOVA test ($p < 0.05$).

Table S1: Blue crab chitosan (Cs) nomenclature and respective acetylation degrees (AD) and average molecular weights (g mol^{-1}).

Cs	—	AD (%)		
		17	**13**	**8**
Cellulase digestion reaction-time (h)	**0**	CsI-0	CsII-0	CsIII-0
	1	CsI-1	CsII-1	CsIII-1
	3	CsI-3	CsII-3	CsIII-3
Cs	—	AD (%)		
		17	**13**	**8**
Digestion reaction-time (h)	**0**	125 600	118 900	115 000
	1	17 800	59 270	78 430
	3	10 440	18 540	16 040

Table S2: Different blue crab chitosan-based hydrogels (GCs) feed compositions and respective nomenclature.

Cs-based hydrogels	3% (w/v) Cs content		
	CsI	CsII	CsIII
Cs-0	GCsI-0	GCsII-0	GCsIII-0
Cs-1	GCsI-1	GCsII-1	GCsIII-1
Cs-3	GCsI-3	GCsII-3	GCsIII-3